Multiscale and Multidisciplinary Modeling, Experiments and Design (2025) 8:411
https://doi.org/10.1007/s41939-025-00968-z

ORIGINAL PAPER

Tri-hybrid nanofluids for thermal applications: stability, magneto-hydrodynamics, and machine learning prediction

Victor O. Adogbeji[1,6] · Emmanuel O. Atofarati[2] · Kuvendran Govinder[1] · Mohsen Sharifpur[1,3,4] · Josua P. Meyer[5]

Received: 24 April 2025 / Accepted: 2 July 2025 / Published online: 11 August 2025

Abstract

This study presents a comprehensive experimental and analytical investigation into the thermophysical and magneto-hydrodynamic (MHD) properties of Fe_3O_4/Al_2O_3/MWCNT/DIW tri-hybrid nanofluids (THNFs) across varying nanoparticle ratios with Sample A (15 wt.% Fe_3O_4, 80 wt.% Al_2O_3, 5 wt.% MWCNT), Sample B (20 wt.% Fe_3O_4, 70 wt.% Al_2O_3, 10 wt.% MWCNT), Sample C (20 wt.% Fe_3O_4, 60 wt.% Al_2O_3, 20 wt.% MWCNT), Sample D (25 wt.% Fe_3O_4, 50 wt.% Al_2O_3, 25 wt.% MWCNT), and Sample E (33.33 wt.% of each material). The effects of temperature (10–50 °C) on viscosity, thermal conductivity (TC), electrical conductivity (EC), stability, and sedimentation were analysed for advanced thermal management applications. Results indicate that the hybridization ratios markedly influence THNF properties. Higher Al_2O_3 content enhances stability by reducing particle agglomeration, while increased Fe_3O_4 and MWCNT fractions elevate EC, however, excessive MWCNT raises viscosity, potentially impacting pumping efficiency. Notably, Sample E offers an optimal balance of TC, stability, and viscosity at lower concentrations. pH measurements reveal an acidic trend that decreases with rising temperature and volume fraction, potentially leading to corrosion in metallic systems. Strategies such as surfactant addition and surface functionalization are proposed to mitigate these effects. Moreover, machine learning models (Gradient Boosting, Random Forest, LightGBM) identified temperature as the dominant factor influencing TC and viscosity, while nanoparticle volume fraction primarily affected pH and EC, achieving high predictive accuracy ($R^2 > 0.96$, MSE < 0.000025).

Keywords Tri-hybrid nanofluids · Thermal conductivity enhancement · Stability and sedimentation analysis · Machine learning prediction · Thermophysical properties · Magneto-hydrodynamics (MHD)

Abbreviations

AL_2O_3	Aluminium oxide nanoparticles
Au	Gold nanoparticles
C_p	Specific heat transfer
Co_2O_3	Cobalt (III) oxide nanoparticles
Cu	Copper nanoparticles
CuO	Copper oxide nanoparticles
CNTs	Carbon nanotubes
DIW	Deionized water
DW	Distilled water
EC	Electrical conductivity
EG	Ethylene glycol
Fe_2O_3	Iron (III) oxide nanoparticles
Fe_3O_4	Iron (IV) oxide nanoparticles

✉ Mohsen Sharifpur
mohsen.sharifpur@up.ac.za

Victor O. Adogbeji
adogbeji.victor@mapoly.edu.ng

[1] Department of Mechanical and Aeronautical Engineering, University of Pretoria, Private Bag X20, Hatfield, Pretoria 0028, South Africa

[2] Department of Mechanical, Bioresources and Biomedical Engineering, University of South Africa, Science Campus, Johannesburg 1710, Florida, South Africa

[3] School of Mechanical, Industrial and Aeronautical Engineering, University of the Witwatersrand, Private Bag 3, Wits 2050, South Africa

[4] Department of Medical Research, China Medical University, China Medical University, Taichung, Taiwan

[5] Department of Mechanical and Mechatronic Engineering, Stellenbosch University, Stellenbosch, South Africa

[6] Department of Mechanical and Industrial Engineering Technology, University of Johannesburg, Johannesburg, Johannesburg, South Africa

G	Gauss
GA	Gum Arabic
GMO	Graphene magnetite oxide
MF	Magnetic fields
MHNFs	Magnetic hybrid nanofluids
MNFs	Magnetic nanofluids
MNPs	Magnetic nanoparticles
MWCNT	Multiwalled carbon nanoparticle
SF	Sedimentation Factor
SiO_2	Silicon oxide nanoparticles
TC	Thermal conductivity
Ti O_2	Titanium oxide nanoparticles
TEI	Total efficiency index
THNFs	Tri-hybrid nanofluids
UV-Vis	Ultra Violet-Visible

Greek symbols

Φ	Volume concentration (vol%)
μ	Viscosity (kg/m.s)
κ	Thermal conductivity (Wm /K-1)
σ	Electrical conductivity (mS/cm $-$ 1)
ρ	Density (Kg /m^3)

Subscripts

avg	Average
bf	Base fluid
n_f	Nanofluid
n_p	Nanoparticles

1 Introduction

Numerous studies have established that traditional fluids like ethylene glycol, glycerol, water, paraffin oil, and oil, possess relatively lower thermal properties compared to solid metals (Wole-osho et al. 2020; Okonkwo et al. 2021). Due to the inherent limitations of traditional heat transfer fluids and the growing need for more effective thermal management solutions in various applications, including advanced cooling systems and next-generation heat exchanger technologies, extensive research efforts have been dedicated to developing innovative alternatives. These advancements have led to the creation of novel thermal fluids with superior thermophysical properties, significantly enhancing heat transfer efficiency. As a result, modern thermal management systems have become not only more effective but also more compact, enabling the design of smaller, more energy-efficient, and high-performance heat exchangers that meet the increasing demands of industrial, automotive, and electronic cooling applications. The concept of enhancing heat transfer fluids can be traced back to the pioneering work of Maxwell (1891), who first introduced the idea of increasing thermal conductivity by incorporating solid particles into base fluids. His study emphasized that non-homogeneous media could lead to variations in thermal conductivity (TC) coefficients and proposed a theoretical model to predict the effective thermal conductivity of such heterogeneous systems. This laid the foundation for further advancements, leading to the development of a more refined approach by Hamilton and Crosser (1962). who introduced an improved model for estimating the thermal and physical properties of fluids containing suspended solid particles.

Although these particle-laden fluids exhibited notable enhancements in thermal performance, experimental investigations uncovered significant challenges that limited their practical applications. Key drawbacks included instability and the lack of uniform particle distribution within the fluid medium, as reported by Sun et al. (2020). And Adio et al. (2025). Additionally, issues such as clogging in flow passages, increased sedimentation, and excessive pumping power requirements were observed, as highlighted by Mehrali et al. (2014), and Zubir et al. (2015). These limitations prompted the search for more efficient thermal fluids that could overcome these setbacks while maintaining superior heat transfer characteristics.

A major breakthrough in this field came with the work of Choi and Eastman (1995). who introduced the revolutionary concept of dispersing nanoscale solid particles into conventional heat transfer fluids, giving rise to what is now known as nanofluids. Unlike their micro-sized counterparts, nanofluids offered several key advantages, including enhanced thermal conductivity, improved stability, and minimal clogging in flow systems. The advent of nanotechnology allowed for the precise control of particle size, shape, and dispersion techniques, leading to more stable suspensions and better heat transfer efficiency without the excessive viscosity and sedimentation issues seen in earlier particle-based fluids.

This innovation has since paved the way for extensive research into hybrid nanofluids, where multiple types of nanoparticles are combined to achieve synergistic effects, further improving thermophysical properties and overall heat transfer performance (Adogbeji et al. 2025a).The continuous evolution of nanofluid technology has enabled the development of more compact and energy-efficient thermal management systems, contributing to advancements in diverse applications, including automotive cooling, electronic heat dissipation, industrial heat exchangers, and renewable energy systems. As research progresses, the optimization of nanoparticle selection, base fluid compatibility, and external field interactions, such as magnetic and electric

fields, continue to refine the capabilities of these next-generation heat transfer fluids (Adogbeji et al. 2024a, 2024b).

Nanofluids have garnered significant interest in recent years due to their potential to greatly improve heat transfer efficiency in various thermal systems. Extensive research has focused on single component nanofluids, which consist of a base fluid combined with one type of nanoparticle (Adogbeji et al. 2025a). Numerous experimental and theoretical studies have confirmed that these nanofluids enhance thermal conductivity and heat transfer performance, positioning them as promising alternatives to traditional fluids used in heat transfer processes. Nanofluids containing nanoparticles such as Al_2O_3, TiO_2, CuO, SiO_2, Fe_3O_4, Fe_2O_3, ZnO, Ag, MgO, carbon nanotubes (CNT), multi-walled carbon nanotubes (MWCNT), and graphene have demonstrated considerable potential in applications like cooling, thermal storage, and energy systems where higher thermal efficiency is essential (Das et al. 2006; Timofeeva et al. 2011). These nanomaterials, spanning metal oxides, carbon-based particles, and metals, offer a wide range of thermophysical properties that make them suitable for improving heat transfer.

Although single component nanofluids show great promise, the pursuit of even more efficient heat transfer fluids has led to the emergence of hybrid nanofluids. These fluids, which blend two different types of nanoparticles such asFe_3O_4/TiO_2, Fe_3O_4/ZnO, Fe_3O_4/MgO, Al_2O_3/MWCNT, and Fe_3O_4/MWCNT and many more are dispersed in traditional based fluid such as water, paraffin oil, ethylene glycol, glycerol, and oil are still undergoing advanced research. Studies have shown that hybrid nanofluids frequently outperform their single-component counterparts due to the synergistic interaction between the nanoparticles(Adogbeji et al. 2025b). The unique thermophysical properties of each type of nanoparticle contribute to improved thermal conductivity, stability, and overall heat transfer performance both in Jet cooling system, natural and forced convention heat transfer.

Building on the success of hybrid nanofluids, tri-hybrid nanofluids (THNFs) have emerged as a groundbreaking advancement in thermal fluid technology. Unlike conventional nanofluids, which utilize a single type of nanoparticle, or hybrid nanofluids, which combine two different nanoparticles, THNFs integrate three distinct nanoparticle types within a base fluid. This multi-component approach offers a highly effective strategy to enhance thermal conductivity, heat transfer efficiency, and overall fluid stability while mitigating the limitations observed in single and binary nanofluid systems.

The justification for developing THNFs lies in the inherent limitations of traditional nanofluids. While mono and hybrid nanofluids have demonstrated significant improvements in heat transfer performance, they often encounter trade-offs between thermal conductivity enhancement, viscosity increase, and particle stability. By incorporating three nanoparticles with complementary properties, THNFs create a synergistic effect that optimizes thermophysical performance across multiple dimensions. For instance, one type of nanoparticle may contribute to superior thermal conductivity (e.g., metallic nanoparticles such as Ag or Cu), while another enhances suspension stability (e.g., oxides like Al_2O_3, TiO_2 or SiO_2), and a third may improve heat absorption and energy transport under varying flow conditions (e.g., magnetic nanoparticles like Fe_3O_4 (magnetite), Fe_2O_3 (hematite)). This tailored combination allows for enhanced heat dissipation while maintaining fluid homogeneity and reducing agglomeration.

Furthermore, the strategic selection of nanoparticles in THNFs enables precise control over viscosity, ensuring that the improved thermal performance does not lead to excessive pressure drops or increased pumping power requirements. Research has also shown that tri-hybrid formulations can be fine-tuned to achieve optimal performance for specific applications, including industrial heat exchangers, solar thermal collectors, automotive cooling systems, and electronic heat sinks (Mousavi et al. 2019; Adun et al. 2021; Ahmad et al. 2023; Sahoo 2020).

Additionally, If the synergistic effect is optimized, THNFs can improve long-term stability compared to their hybrid counterparts due to more effective surfactant interactions and reduced sedimentation rates. This is particularly beneficial in practical applications where consistent thermal performance over extended operational periods is critical. The integration of tri-hybrid nanofluids into advanced thermal management systems signifies a major step forward in achieving next-generation heat transfer fluids with unprecedented efficiency, paving the way for more compact, energy-efficient, and high-performance thermal systems across multiple industries.

Building on the advancements of hybrid nanofluids, THNFs have naturally emerged as the next step in optimizing thermal performance. These fluids incorporate three distinct types of nanoparticles, offering a novel strategy to further improve heat transfer capabilities. The nanoparticle combinations often include either metals such as silver (Ag), copper (Cu), aluminum (Al), iron (Fe), gold (Au); or metallic oxides like copper oxide (CuO) and aluminum oxide (Al_2O_3); carbide ceramics such as silicon carbide (SiC) and titanium carbide (TiC); semiconductors like titanium dioxide (TiO_2) and silicon dioxide (SiO_2); or carbon-based materials like nano-diamond and graphite; as well as carbon nanotube variations, including carbon nanotubes (CNT), multi-walled carbon nanotubes (MWCNT) single-walled (SWCNT), and double-walled (DWCNT) carbon nanotubes.

By leveraging the magnetic properties of Fe_3O_4, the thermal stability of Al_2O_3, the high thermal conductivity of MWCNTs, and potentially other nanoparticles like TiO_2 or Ag, these THNFs can offer significantly enhanced thermal performance, surpassing both single-component and hybrid nanofluids (Adun et al. 2021).

Researchers must thoroughly understand the distinct properties of each nanoparticle within the various nanoparticle groups in order to effectively combine them for specific thermal management applications. Each nanoparticle offers unique thermophysical characteristics such as magnetic, thermal, or conductive properties that can significantly influence the overall performance of the nanofluid. By strategically selecting and combining nanoparticles based on their individual strengths, researchers can tailor trihybrid nanofluids to meet the precise requirements of a given application, optimizing heat transfer, stability, and efficiency. This advancement is particularly promising for applications in heat transfer, cooling systems (Ramadhan et al. 2019, 2020), and thermal storage, where maximizing efficiency is critical (Ahmad, et al. 2023; Muzaidi et al. 2021).

Adun et al. (Adun et al. 2021) conducted an experimental analysis to evaluate the specific heat capacity of water-based $Fe_3O_4/Al_2O_3/ZnO$ ternary hybrid nanofluids. Three mixture ratios were prepared: 1:1:1 (33.33% Fe_3O_4, 33.33% Al_2O_3, 33.33% ZnO), 1:2:1 (25% Fe_3O_4, 50% Al_2O_3, 25% ZnO), and 1:1:2 (25% Fe_3O_4, 25% Al_2O_3, 50% ZnO) at volume fractions of 0.5%, 0.75%, 1%, and 1.25%. The experiments were conducted within a temperature range of 25 °C to 65 °C. Zeta potential and particle size measurements were used to evaluate nanoparticle dispersion and stability, while high-resolution scanning electron microscopy (SEM) was employed to examine the nanocomposite's morphological structure. Results showed a direct correlation between temperature and specific heat capacity, with the specific heat capacity decreasing as the volume concentration increased. Maximum increases in specific heat capacity of 11.94%, 14.65%, and 13.56% were recorded for the 1:1:1, 1:2:1, and 1:1:2 mixtures, respectively, at a volume concentration of 1.25% and 25 °C, relative to the base fluid. A peaking effect was observed in the 1:1:1 ratio, while the lowest specific heat capacity was recorded for the 1:2:1 mixture.

Sepehrnia et al. (2023) and Kanti et al. (2022) both conducted in-depth experimental studies on the thermophysical behavior of graphene oxide-based hybrid nanofluids, emphasizing their potential for thermal applications. Sepehrnia et al. (2023) explored the dynamic viscosity of hydraulic oil HLP 68-based ternary hybrid nanofluids (Fe_3O_4, TiO_2, GO) across varied mixing ratios (1:1:1 to 2:1:1), solid volume fractions (0–1%), and temperatures (15–65 °C), confirming Newtonian behavior with viscosity enhancements reaching up to 1990% at 15 °C. Zeta potential and DLS analyses verified high colloidal stability, particularly for the 2:1:1 mixture. Additionally, a subtractive clustering-based ANFIS model demonstrated exceptional predictive accuracy ($R^2 >$ 0.999). Complementarily, Kanti et al. (2022) synthesized GO, SiO_2, and TiO_2 nanoparticles to formulate mono and hybrid nanofluids (GO- SiO_2, GO- TiO_2) using PVP as a stabilizer. Evaluated over a 0.05–1.0% concentration range and 30–60 °C, GO nanofluids exhibited the highest viscosity (127% above SiO_2) and superior thermal conductivity—up to 14.4% greater than GO- SiO_2 at 60 °C. Their findings confirmed long-term dispersion stability and highlighted the improved thermal efficiency of hybrid nanofluids at elevated temperatures (> 45 °C). Together, both studies underscore the critical role of nanoparticle composition, temperature, and surfactant optimization in tuning the rheological and thermal behavior of nanofluids for advanced heat transfer applications.

Also, Mousavi et al. (2019) investigated the influence of nanoparticle volume concentration and temperature on the thermophysical properties and rheological behavior of $CuO/MgO/TiO_2$ based ternary hybrid nanofluids. Five distinct types of these nanofluids were synthesized with varying mass ratios of CuO, MgO, and TiO_2. The compositions included: Sample A (33.3 wt.% CuO, 33.3 wt.% MgO, 33.3 wt.% TiO_2), Sample B (50 wt.% CuO, 25 wt.% MgO, 25 wt.% TiO_2), Sample C (60 wt.% CuO, 30 wt.% MgO, 10 wt.% TiO_2), Sample D (25 wt.% CuO, 50 wt.% MgO, 25 wt.% TiO_2), and Sample E (25 wt.% CuO, 25 wt.% MgO, 50 wt.% TiO_2). The experimental conditions ranged from 15 to 60 °C, with solid volume concentrations between 0.1% and 0.5%. Their findings indicated that both temperature and nanoparticle concentration significantly affected the properties of the ternary hybrid nanofluids. All samples exhibited Newtonian behavior. As the nanoparticle concentration and temperature increased, so did thermal conductivity and dynamic viscosity, with type C showing the highest increase. Specific heat capacity showed a decreasing trend up to 35 °C, after which it increased with temperature. The researchers developed four empirical correlations to predict viscosity, thermal conductivity, specific heat capacity, and density for these nanofluids.

Muzaidi et al. (2021) investigated $CuO/SiO_2/TiO_2$ trihybrid nanofluids, analysing parameters such as density, crystallite size, and surface morphology. Their findings indicated that density increased with volume concentration, with sample t1 achieving a peak density of 2.26 g/mL. X-ray diffraction (XRD) confirmed successful trihybrid formation through distinct diffraction peaks for CuO, TiO_2, and SiO_2, while crystallite size calculations revealed reduced dimensions (~ 5.2 nm), further supported by SEM images displaying fine particle dispersion. Sample t1, having the highest concentration, also delivered the best thermal output (~ 55 °C) under solar exposure, underscoring the significance of concentration on thermal enhancement.

Building on this foundation, the present study was undertaken to systematically address existing gaps in understanding the thermophysical behavior of trihybrid nanofluids, specifically targeting industrial thermal management systems such as cooling units, heat exchangers, and energy devices. While previous studies explored various trihybrid

combinations, the interplay between nanoparticle composition, stability, and performance under dynamic operating conditions remains underexplored.

This study focuses on Fe_3O_4/Al_2O_3/MWCNT-based deionized water (DIW) trihybrid nanofluids, selected due to their complementary properties of Fe_3O_4 contributes magnetic and thermal responsiveness, Al_2O_3 ensures colloidal stability, and MWCNTs offer high thermal conductivity. These materials were strategically chosen to address the current trade-off between thermal conductivity enhancement and viscosity increase an issue that often limits the practical adoption of nanofluids in real-world systems. To investigate this, five distinct mixing ratios Sample A (15:80:5), Sample B (20:70:10), Sample C (20:60:20), Sample D (25:50:25), and Sample E (33.33% each by weight) were designed to study the effect of varying nanoparticle contributions on stability and thermophysical behavior. These ratios were selected to span a practical range of concentrations from 0.00625 to 0.3 vol.%, allowing the identification of an optimal formulation that maximizes heat transfer with minimal viscosity penalties.

Comprehensive experimental evaluations were conducted, including UV–Vis spectrophotometry for dispersion stability, pH and electrical conductivity measurements, and temperature-dependent assessments of viscosity and thermal conductivity. To accelerate formulation optimization and reduce reliance on exhaustive experimental trials, a machine learning (ML) model was developed. Using regression-based algorithms, the model was trained on experimental inputs nanoparticle composition, volume fraction, and temperature to predict thermal conductivity and viscosity. This approach enables data-driven selection of nanofluid formulations tailored for specific industrial needs. The novelty of this work lies in (i) the strategic combination of metallic (Fe_3O_4, Al_2O_3) and carbonaceous (MWCNT) nanoparticles to synergistically enhance heat transfer; (ii) the systematic evaluation of mixture ratios to resolve the conductivity-viscosity trade-off; and (iii) the integration of machine learning for predictive modeling and rapid optimization. By advancing the understanding of Fe_3O_4/Al_2O_3/MWCNT trihybrid nanofluids and demonstrating their potential under realistic thermal operating conditions, this study offers a promising pathway toward next-generation, energy-efficient thermal management fluids.

2 Experimental methodology

2.1 Nanofluids preparation and materials

In this research, Fe_3O_4,Al_2O_3, and MWCNT tri-hybrid ferrofluids dispersed in deionized water were synthesized using a two-step method, yielding volume fractions ranging from 0.3 vol.%. The hybridization mixing ratios (HMR) of Iron III Oxide (Fe_3O_4),Al_2O_3, and MWCNT were varied, and the thermophysical properties of both the nanoparticles and the base fluid are detailed in Table 1. Meanwhile, Table 2 presents the composition of **Samples A**, **B, C, D,** and **E**, which were prepared for heat transfer experiments. To disperse the nanoparticles in water, the mixture was first stirred with mechanically powered stirrer and then subjected to 100% amplitude ultrasonication for four hours. The sonication process was conducted at a controlled bath temperature of 20 °C. Gum Arabic was used as a surfactant at a weight ratio of 0.5% to stabilize the THNFs tri-hybrid nanofluids. Equations 1 and 2 (Adun et al. 2021) were applied to determine the volume concentration for all the nanofluids. Figure 1 illustrates the process visually.

Physical assessments, including measurements of viscosity and stability, are conducted over time at a controlled at 25 °C, with monitoring extending for up to 12 h and a month. Visual inspections and stability tests are also performed, with Fig. 1 illustrating key aspects of the process **(a)** a schematic diagram outlining the steps involved in the preparation of THNFs, and **(b–d)** a visual representation of the nanofluid stability after 24 h post-preparation for samples. This rigorous preparation and assessment protocol ensures the thorough evaluation of the nanofluids' performance and stability over time for all samples are evaluated.

$$\varphi = \left(\frac{Y_{Fe_3O_4}\left(\frac{W}{\rho}\right)_{Fe_3O_4} + Y_{Al_2O_3}\left(\frac{W}{\rho}\right)_{Al_2O_3} + Y_{MWCNT}\left(\frac{W}{\rho}\right)_{MWCNT}}{Y_{Fe_3O_4}\left(\frac{W}{\rho}\right)_{Fe_3O_4} + Y_{Al_2O_3}\left(\frac{W}{\rho}\right)_{Al_2O_3} + Y_{MWCNT}\left(\frac{W}{\rho}\right)_{MWCNT} + \left(\frac{W}{\rho}\right)_{DIW}} \right) \quad (1)$$

$$\rho_{Fe_3O_4/Al_2O_3/MWCNT} = \frac{\left(\rho_{Fe_3O_4} \times W_{Fe_3O_4}\right) + \left(\rho_{Al_2O_3} \times W_{Al_2O_3}\right) + \left(\rho_{MWCNT} \times W_{MWCNT}\right)}{W_{Fe_3O_4} + W_{Al_2O_3} + W_{MWCNT}} \quad (2)$$

where the nanoparticle type ratio of each is depicted by Y and W nanoparticle mass.

2.2 Sample Preparation and stability testing using UV–visible spectrophotometry.

The samples were analyzed using UV–visible spectrophotometry (Thermo Scientific Multiskan Go) at a controlled room temperature of 24.8 °C, with distilled water serving as

Table 1 Physical characteristics of the materials under study at room temperature

Thermophysical property	Nanoparticle	Supplier value	Particle size (nm)	Supplier	Purity	Shape
Thermal conductivity (W/mK)	Fe_3O_4	80.4	(20–30 nm)	Nanostructured and Amorphous Material Inc., USA	99%	Plate-like nanosheet
	Al_2O_3	37	(20–30 nm)		99%	Spherical
	MWCNT	3000	(7 nm)		> 95	
	DIW	0.613				
Specific heat (J/kg.K)	Fe_3O_4	670				
	Al_2O_3	765	–	–	–	–
	MWCNT	711				
	DIW	4179				
Density (kg/m^3)	Fe_3O_4	5180				
	Al_2O_3	3960	–	–	–	–
	MWCNT	2100				
	DIW	997				
Dispersant Gum Arabic	Gum Arabic	–	–	Sigma-Aldrich, Germany	–	–

Reference: Material specifications provided by Nano Research Materials Inc. (USA) (US4314)

Table 2 Hybridization ratio of Fe_3O_4/Al_2O_3/MWCNT/DIW try-hybrid nanofluids

Samples	Fe_3O_4	Al_2O_3,	MWCNT	Concentration	Hybridization Ratio (Fe_3O_4 : Al_2O_3 : MWCNT)
A	15	80	5	0.3	15%: 80%: 5%
B	20	70	10	0.3	20%: 70%: 10%
C	20	60	20	0.3	20%: 60%: 20%
D	25	50	25	0.3	25%: 50%: 25%
E	33.33	33.33	33.33	0.3	33.33%: 33.33%: 33.33%

the reference medium as illustrated in Fig. 2b. Each sample was measured six times to ensure accuracy, and the mean values were used for the final analysis. The sedimentation factor for each sample was calculated based on Eq. 3 (Adogbeji et al. 2025a), which quantifies the percentage of sedimentation in the nanofluids.

Light spectrum measurements were taken over a broad range, from 200 to 1000 nm. The spectrum was scanned with 100 nm intervals between 200 and 700 nm, and with finer 50 nm intervals from 750 to 1000 nm, to capture a detailed absorbance profile. These absorbance readings across the specified wavelength ranges allowed for the analysis of the stability and dispersion quality of the THNFs.

By comparing the absorbance values across the different wavelengths, the percentage of sedimentation was calculated, offering insights into the stability of the nanofluids over time. This method ensures a thorough evaluation of the dispersion characteristics and particle stability within the nanofluids, providing critical data on their long-term usability and effectiveness for various thermal applications. The calculation of sedimentation factor using Eq. 3 further highlights the sedimentation behavior, which is an important indicator of the overall stability of the tri-hybrid nanofluids.

$$\text{Sedimentation factor (SF)} = \left(\frac{Maximum\ absorbance - Total\ average\ absorbance}{\text{Maximum absorbance}}\right) \times 100 \quad (3)$$

2.3 Sample preparation and imaging procedure for SEM analysis of nanoparticles

For the SEM imaging sample preparation, aluminium stubs were used as holders, onto which carbon tape was applied. The nanoparticles were then carefully spread over the carbon tape. After this, the aluminium stubs were mounted onto a Quorum Q1556 S/E/ES carbon coater, as shown in Fig. 2c, and the nanoparticles were coated with a thin layer of carbon to enhance conductivity. Once the carbon coating process

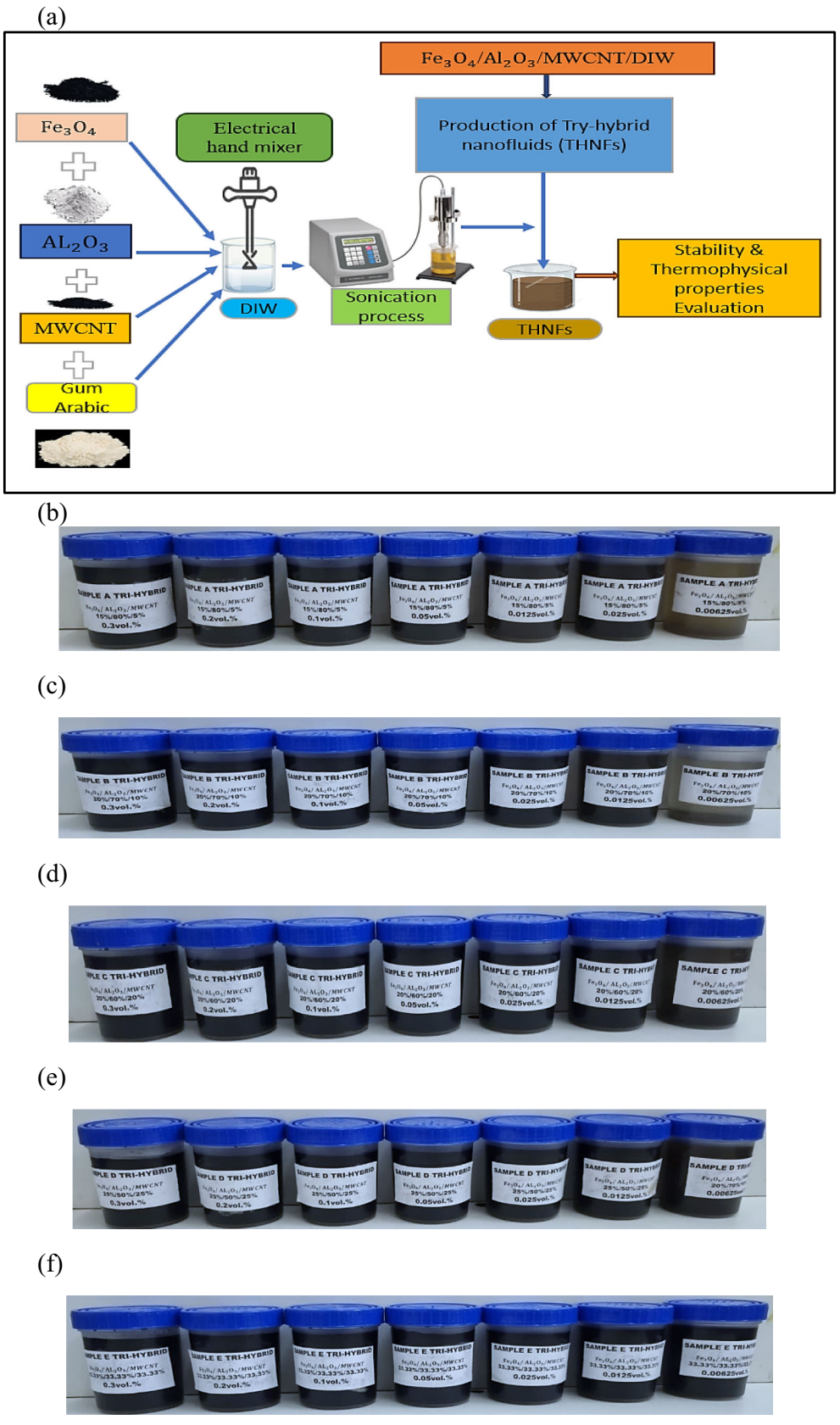

Fig. 1 **a** Schematic diagram of the preparation process for THNFs, **b** a visual representation of the nanofluid stability after 24 h post-preparation for all samples

Fig. 2 Samples of equipment used **a** Ultrasonicator, **b** spectrophotometry, **c** carbon coater, **e** SEM microscopy, **d** X-ray diffractometer

was completed, the sample was transferred to the Zeiss Crossbeam 540 field emission gun scanning electron microscope (FEG-SEM), as shown in Fig. 2d. The sample was carefully mounted onto the microscope stage, and the vacuum system was activated. The focus lens was adjusted to ensure a sharp image of the nanoparticles without visible stretching.

The process was repeated as needed to avoid blurred images until a clear and focused image was obtained. The central area of interest was captured to provide a clear representation of the nanoparticle structure, ensuring a balanced grayscale for accurate visualization. Images were captured at various magnifications of 20, 50, and 100 k, for each sample. This multi-magnification approach allowed for a comprehensive comparison of the nanoparticle structures at different scales, enhancing the SEM procedure's effectiveness in visualizing the detailed morphology of the nanoparticles.

2.4 XRD Procedure for characterizing, Fe_3O_4, Al_2O_3, and MWCNT nanoparticles

For the physical characterization of Al_2O_3, MWCNT and Fe_3O_4 nanoparticles, an advanced D8 X-ray diffractometer was employed illustrated in Fig. 2e. The samples were carefully ground using an agate mortar and pestle, then transferred to a sample holder with a diameter of 1.5 cm and a thickness of 1 mm. A glass plate was used to ensure the sample surface was flat within the holder. The samples were positioned in front of the X-ray beam, and the stage was rotated to ensure uniform exposure to the beam. To control the X-ray beam's divergence, a V20 slit variable was employed before it reached the sample. The radiation from the X-ray source (CuKα, 1.54056 Å) was diffracted by the sample and recorded by the detector. The experiment was conducted with

a tube voltage of 40 kV and a current of 40 mA. A scanning rate of 2 degrees per minute was used due to the small size of the samples. All diffraction measurements were performed at room temperature within a 25° to 60° range, and the results were plotted using Origin software.

2.5 Measurement of thermal and physical properties (pH, electrical conductivity (EC), density, viscosity (μ), and thermal conductivity (TC)

Measuring pH, electrical conductivity (EC), density, viscosity, and thermal conductivity (TC) is crucial for assessing the efficiency and stability of nanofluids in heat transfer applications. TC determines a fluid's ability to transfer heat, directly impacting cooling performance. μ influences flow behavior and pumping power, where excessive viscosity increases frictional resistance, reducing efficiency. Density affects mass flow rates and pressure drop, playing a key role in system design. EC indicates charge-carrying capacity, which can enhance nanoparticle dispersion and enable electromagnetic control in heat transfer systems. pH stability is essential to prevent nanoparticle agglomeration, ensuring consistent thermal performance. Accurate characterization of these properties allows for optimized nanofluid formulations, improving heat transfer efficiency and system reliability.

2.5.1 Measurement of electrical conductivity and pH of THNFs

The EC meter was initially calibrated using the standard calibration fluid provided by the manufacturer. Upon calibration, the standard fluid was measured at 25 °C (in triplicate), yielding an average value of 1413.6 $\mu S \cdot cm^{-1}$. After calibration, the electrical conductivity of deionized water and tri-hybrid nanofluids was measured at temperatures ranging from 10 to 50 °C, with readings taken at 5 °C intervals. The EC of THNFs improvement was determined by Eq. 4.

The pH meter was calibrated using buffer solutions with pH values of 4, 7, and 10. Following this, the pH levels of the hybrid nanofluids were measured as illustrated in Fig. 3a.

$$\%EC_{improvement} = \left(\frac{EC_{nf} - EC_{bf}}{EC_{bf}}\right) \times 100 \tag{4}$$

2.5.2 Measurement of density THNFs

The density of the trihybrid nanofluid was measured using a Radwag PS750 R2 balance (sensitivity 0.001 g, linearity ± 3 mg) and a corked glass pycnometer with a fixed volume of 50.448 cm^3. The density was calculated by dividing the mass of the filled pycnometer by its volume. Each measurement was repeated three times, and the average result was used as illustrated in Fig. 3b

For accurate measurements, nanofluid samples were placed in labelled holders and submerged in a thermal bath set to the desired temperature, with thermal equilibrium confirmed using a mercury thermometer. After reaching equilibrium, the samples were carefully transferred to the cleaned, dried density bottle. The bottle was filled to one-third capacity with the nanofluid, and the stopper was inserted, allowing excess liquid to escape. The filled bottle was then submerged in the thermal bath to maintain the desired temperature, and any displaced liquid was removed with tissue. Finally, the density bottle was weighed on an analytical balance to determine the nanofluid's density. This process was repeated three times for each sample, and the average of the results was used. The data collected were then analysed.

The density of the fluid was calculated by determining its mass and using the fixed volume of a pycnometer. The relationship among the measured mass (m), density of the THNFs (ρ), and the known volume of the pycnometer (V) is expressed in Eq. 5.

$$\boldsymbol{\rho} = \frac{\boldsymbol{m}}{\boldsymbol{V}} \tag{5}$$

Uncertainty analysis for the measured mass and computed density was performed following the methodology outlined by Atofarati et al. (2023), Moffat (1988) and Kline (1985). The estimation of δx_i for each parameter considered both bias (b) and precision (p) errors using Eq. 6 and the uncertainty was calculated using Eq. 7. This analysis utilized the"Uncertainty"function in Python, which computes uncertainties with a 95% confidence interval. The uncertainty in the mass measurement was ± 3.17 mg, while the uncertainty in the density calculation was ± 0.000022 g/cm^3.

$$\mathbf{x_i} = \left(\mathbf{b_i^2} + \mathbf{p_i^2}\right)^{1/2} \tag{6}$$

$$\mathbf{D} = \left\{\left(\frac{\mathbf{D}}{\mathbf{x}_1}\right)^2 \partial \mathbf{x}_1 + \left(\frac{\mathbf{D}}{\mathbf{x}_2}\right)^2 \partial \mathbf{x}_2\right\}^{1/2} \tag{7}$$

2.5.3 Measurement of viscosity (μ)

Prior to measuring the viscosity of deionized water and Fe_3O_4/Al_2O_3/MWCNT-DIW THNFs at temperatures ranging from 10 to 50 °C, the vibro-viscometer (SV-10A series, A&D, Tokyo, Japan) was calibrated. A percent error of 1.1% was identified when comparing the measured μ of DIW to its standard reference value.

To ensure precise temperature regulation during the experiment, the vibro-viscometer jacket was integrated with a programmable water bath (LAUDA, Berlin, Germany, model

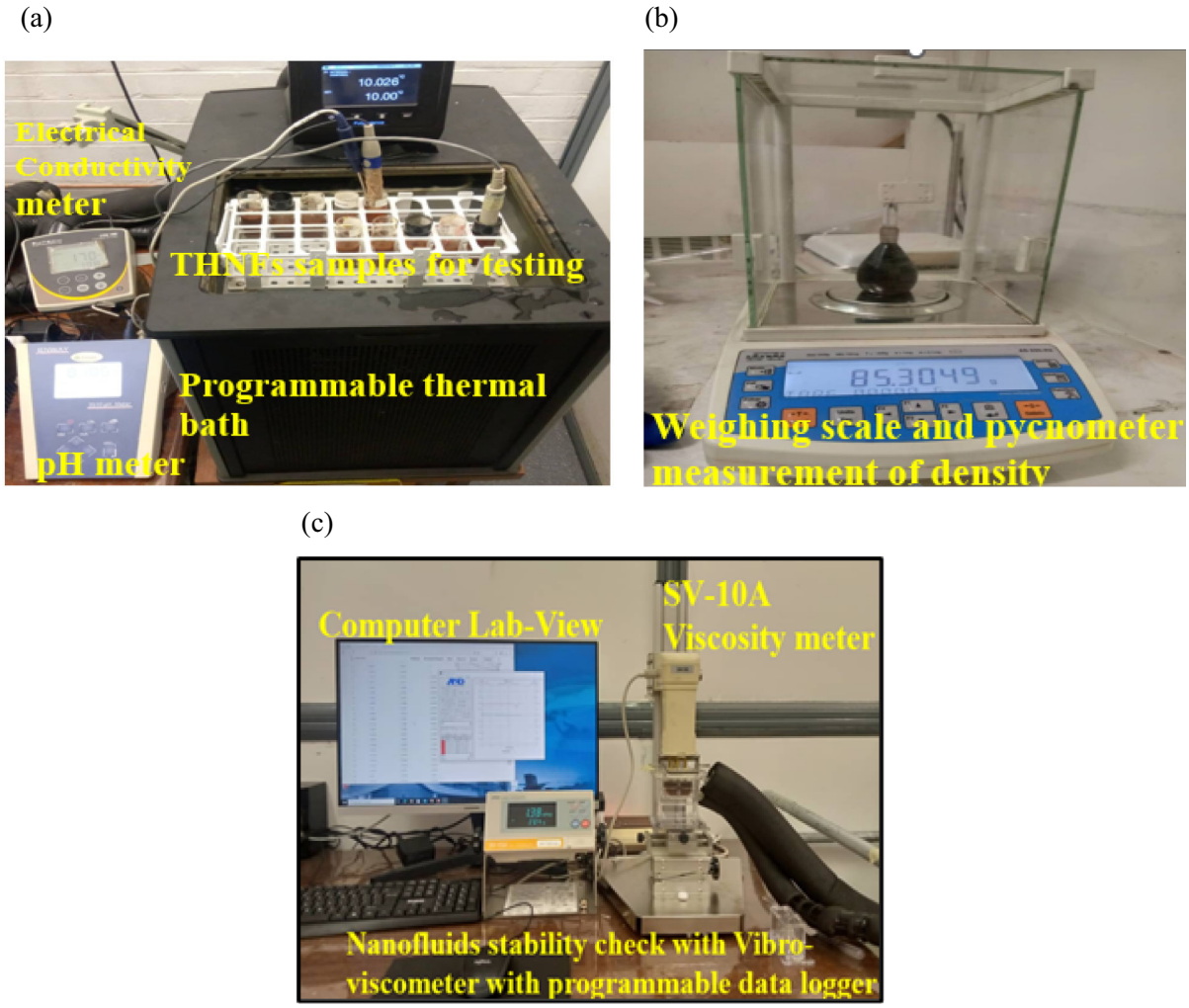

Fig. 3 Measurement equipment used: **a** Electrical and pH meter with thermal bath, **b** pycnometer and weighting scale, **c** data logger with SV-10A Vibro-viscomete

ECO RE1225) and a data logger, as illustrated in Fig. 3c. The obtained data were subsequently processed and analysed.

The μ of THNFs improvement was determined by Eq. 8.

$$\%\mu_{improvement} = \left(\frac{\mu_{nf} - \mu_{bf}}{\mu_{bf}}\right) \times 100 \tag{8}$$

2.5.4 Thermal conductivity measurements (TC)

Prior to conducting measurements, the thermal conductivity device was calibrated using a reference thermal conductivity fluid (glycerine). Following calibration, the TC of deionized water was recorded over a temperature range of 10–50 °C and compared with the reference values reported by Yunus & Ghajar (Çengel et al. 2020). The thermal conductivity of Fe_3O_4/Al_2O_3/MWCNT-DIW THNFs was then measured within the same temperature range. Each measurement was performed six times, and the average values were used for analysis.

A KD2 Pro thermal properties measurement system, manufactured by Decagon Devices Inc., USA, was employed for these measurements. This device operates within a thermal conductivity range of 0.02–2 $W{\cdot}m^{-1}{\cdot}K^{-1}$, with a manufacturer-stated uncertainty of 5%. For accurate readings, at least 15 mm of the sample was required to be positioned parallel to the sensor in all directions, as the sensor emits a heat pulse during measurement.

The nanofluid samples, labelled Sample A to Sample E, corresponded to different nanoparticle volume fractions. The KD2 Pro utilizes the transient hot-wire method to determine thermal conductivity and consists of a handheld controller along with various sensor needles. The KD 2 sensor needle, which has an accuracy of 5%, was specifically used for measuring the thermal conductivity of THNFs.

The Tc of THNFs improvement was determined by Eq. 9.

$$\%K_{improvement} = \left(\frac{K_{nf} - K_{bf}}{K_{bf}}\right) \times 100 \quad (9)$$

2.6 Machine learning analysis

The study employed machine learning techniques to predict both classification and regression-based outcomes using a dataset comprising independent variables: Temperature (T), Volume Fraction (ϕ), Percentage Iron (III) Oxide Nanoparticles (F), Percentage Aluminum (III) Oxide Nanoparticles (A), and Percentage Multiwall Carbon Nanotube Nanoparticles (M). For the classification task, the dependent variable was transformed into a binary outcome using the median threshold, while for the regression task, the study aimed to predict continuous variables such as Viscosity (μ), Thermal Conductivity (K). Similar approach using machine learning to predict the thermophysical properties of hybrid nanofluid and there thermal performance have been implemented in the studies by Atofarati et al. (2025c, 2025), Shahsava et al. (2024, 2023), Kanti et al. (Vicki Wanatasanappan et al. 2023; Kanti et al. 2024) and Sepehrnia et al. (2023a, b).

The dataset underwent preprocessing, including numerical consistency checks, handling missing values using mean imputation, normalization for regression models, and an 80%−20% training–testing split. Machine learning models employed included Support Vector Machine (SVM) with a linear kernel, Random Forest, Gradient Boosting, Logistic Regression, and LightGBM for classification tasks, while multiple linear regression was used for regression predictions. Model evaluation metrics varied based on the task: classification models were assessed using accuracy scores, whereas regression models were evaluated using Mean Squared Error (MSE) and the coefficient of determination (R^2). Additionally, feature importance was analysed using permutation importance to identify key influencing variables across models.

2.7 Uncertainty analysis

The approach outlined in Kulkarni et al. (2008) was utilized to estimate the uncertainty associated with key measured parameters, including dynamic viscosity (μ) and standard deviation (σ), by applying Eqs. (9) and (10). These uncertainties were determined with a 95% confidence level. Instrument precision was assessed based on bias errors, which reflect the accuracy limitations specified by the equipment manufacturer. The uncertainty in viscosity measurements was found to be ± 1.93%, while that of electrical conductivity measurements was ± 2.19%.

$$U_\mu = \sqrt{\left(\frac{\Delta m}{m}\right)^2 + \left(\frac{\Delta V}{V}\right)^2 + \left(\frac{\Delta T}{T}\right)^2 + \left(\frac{\Delta \mu}{\mu}\right)^2} \quad (9)$$

$$U_\sigma = \sqrt{\left(\frac{\Delta m}{m}\right)^2 + \left(\frac{\Delta V}{V}\right)^2 + \left(\frac{\Delta T}{T}\right)^2 + \left(\frac{\Delta \sigma}{\sigma}\right)^2} \quad (10)$$

3 Results and discussion

3.1 Structural and morphological analysis of nanoparticle

The morphological characteristics of Fe_3O_4, Al_2O_3, and MWCNT nanoparticles were investigated using field-emission scanning electron microscopy (FEG-SEM, Zeiss Crossbeam 540). As shown in Fig. 4, Fe_3O_4 nanoparticles appeared spherical with evident clustering, while Al_2O_3 particles formed densely packed spherical agglomerates. MWCNTs exhibited a uniform cylindrical morphology resembling entangled chains. In the trihybrid formulation (Fe_3O_4/Al_2O_3/MWCNT/DIW), Al_2O_3 nanoparticles were observed to adhere along the surface of Fe_3O_4 clusters and MWCNT chains, forming an interconnected network. This structure may enhance thermophoretic and electrophoretic effects when dispersed in fluids, potentially improving thermal and electrical transport, in agreement with prior morphological studies.

3.2 X-ray diffraction (XRD) analysis for structural characterization of Fe_3O_4, Al_2O_3, and MWCNT nanoparticles

X-ray diffraction (XRD) analysis was performed to determine the crystallographic structure and estimate the crystallite size of the individual nanoparticles as shown In Fig. 5. MWCNTs exhibited characteristic peaks at $2\theta = 25.96°$ and 43.1°, corresponding to the (002) and (100) planes of a hexagonal graphite lattice (JCPDS card No. 96-101-1061), confirming a hexagonal $P6_3mc$ structure with lattice parameters a = b = 2.47 Å, c = 6.79 Å. The calculated average crystallite size was 16.7 nm, consistent with Khedaer et al. (2021).

Fe_3O_4 nanoparticles showed peaks at $2\theta = 30.1°$, 35.4°, 43.1°, 53.7°, 56.9°, 62.8°, and 74.5°, indexed to the (220), (311), (400), (422), (511), (440), and (533) planes of a cubic inverse spinel structure (JCPDS No. 19–0629), with an average crystallite size of 14.8 nm. Similarly, Al_2O_3 displayed distinct peaks at $2\theta = 25.6°, 35.1°, 37.8°, 43.3°, 52.6°, 57.5°,$

61.1°, 67.1°, and 77.1°, corresponding to (012), (104), (110), (113), (024), (116), (122), (214), and (119) planes of a hexagonal R-3c structure (ICDD card No. 00–010-0173), yielding a crystallite size of 25.7 nm. Minor additional peaks were attributed to impurity phases. Crystallite sizes were computed using the Debye–Scherrer equation:

$$D = \frac{K\lambda}{\beta\cos\theta} \tag{11}$$

where θ is the Bragg's diffraction angle in radians, λ represents the X-ray wavelength ($\lambda = 1.5406$ ˚A), β is the full width at half maximum (FWHM) in radians, κ is the Scherrer constant (typically equal to 0.9), and D is the average crystallite size. The calculated average crystallite sizes of MWCNT, Fe_3O_4, and Al_2O_3 were observed to be 31.9 nm, 14.8 nm, and 25.7 nm, respectively. Zhuang et al. (2015), and Mohammed et al. (2020) presented similar results on these nanoparticles.

3.3 Stability analysis at different concentrations and hybridization for samples

The stability of Fe_3O_4/Al_2O_3/MWCNT/DIW trihybrid nanofluids (THNFs) was evaluated using UV–Vis spectrophotometry and sedimentation testing across different hybridization ratios (Samples A–E) and volume fractions (0.00625%–0.3%) based on existing methodology in literature (Arifutzzaman et al. 2019; Aravind et al. 2011). Agglomeration due to dominant van der Waals forces and Brownian motion compromises nanofluid stability, especially at high concentrations (Adun et al. 2021; Sahoo 2020). Sedimentation testing, widely employed for nanofluid stability assessment (Chakraborty et al. 2018a, b; Chakraborty and Panigrahi 2020) revealed that lower volume fractions significantly improve dispersion stability.

Table 3 and Fig. 6a–e shows the sedimentation factor (SF), where higher SF values indicate enhanced stability. Sample A (15% Fe_3O_4, 80% Al_2O_3, 5% MWCNT) exhibited the highest SF (89.56%) at 0.00625% vol., decreasing to 12.39% at 0.3% vol., reflecting greater sedimentation at higher concentrations. Samples B through E followed similar trends, with SFs ranging from 88.27% to 74.02% at the lowest volume fraction and dropping to 11.32%–9.04% at 0.3% vol. Sample E (equal distribution of all constituents) showed the lowest stability, suggesting that excessive Fe_3O_4 loading increases sedimentation. These results confirm that hybridization ratio and nanoparticle loading significantly influence nanofluid stability, with Sample A showing the most favorable behavior.

UV–Vis spectrophotometric analysis at 600 nm (Fig. 6f) corroborated sedimentation results. At 0.3% vol., all samples exhibited high absorbance (3.9564–3.9782), indicating dense nanoparticle concentration and increased light attenuation. As volume fraction decreased, absorbance also dropped. Sample A maintained relatively high absorbance even at lower concentrations (0.1249 at 0.00625%), aligning with its superior SF and indicating excellent dispersion stability. In contrast, Samples D and E showed lower absorbance at lower concentrations (e.g., 0.4531 and 0.723 at 0.00625%), suggesting reduced particle density but more uniform dispersion.

Notably, Sample A retained consistent stability across concentrations, while Samples B and C demonstrated strong performance only at very low concentrations. Samples D and E exhibited improved stability at ultra-low volume fractions but became unstable at moderate concentrations. These findings confirm that optimal nanoparticle dispersion occurs at 0.00625%–0.0125% vol., consistent with prior studies (Adogbeji et al. 2025a, 2024b, 2025b), where lower concentrations enhanced heat transfer without incurring flow resistance or pump power penalties.

Overall, the stability trends underscore the critical role of hybridization ratio and concentration. Lower nanoparticle loading not only improves sedimentation resistance and optical dispersion but also minimizes production cost, making such THNFs more viable for real-world heat transfer applications.

3.4 Electrical conductivity and thermal management implications of THNFs

3.4.1 Experimental results for electrical conductivity

The electrical conductivity (EC) of Fe_3O_4/Al_2O_3/MWCNT-based nanofluids was investigated as a function of nanoparticle composition, concentration, and temperature (10–50 °C), as shown in Fig. 7a–e. EC plays a critical role in thermal management, particularly in systems integrating conductive nanoparticles. Deionized water (DIW) served as the base fluid, with nanofluids synthesized at various volume fractions (0.00625–0.3%) and hybridization ratios (Samples A–E). A general increase in EC was observed with rising nanoparticle concentration across all samples. This enhancement is attributed to the intrinsic conductive properties of Fe_3O_4 and MWCNTs. Fe_3O_4 provides magnetic responsiveness, while MWCNTs offer high electrical conductivity due to their high aspect ratio and capacity to form conductive percolation networks. In contrast, Al_2O_3 is electrically insulating and thus reduces the overall EC when present in higher proportions.

Specifically, Sample A (15% Fe_3O_4, 80% Al_2O_3, 5% MWCNT) exhibited moderate EC gains, limited by the dominant presence of Al_2O_3 (Fig. 7a). Sample B (20% Fe_3O_4, 70% Al_2O_3, 10% MWCNT) showed increased EC (Fig. 7b), while Sample C (20% Fe_3O_4, 60% Al_2O_3, 20% MWCNT) demonstrated further improvement due to higher

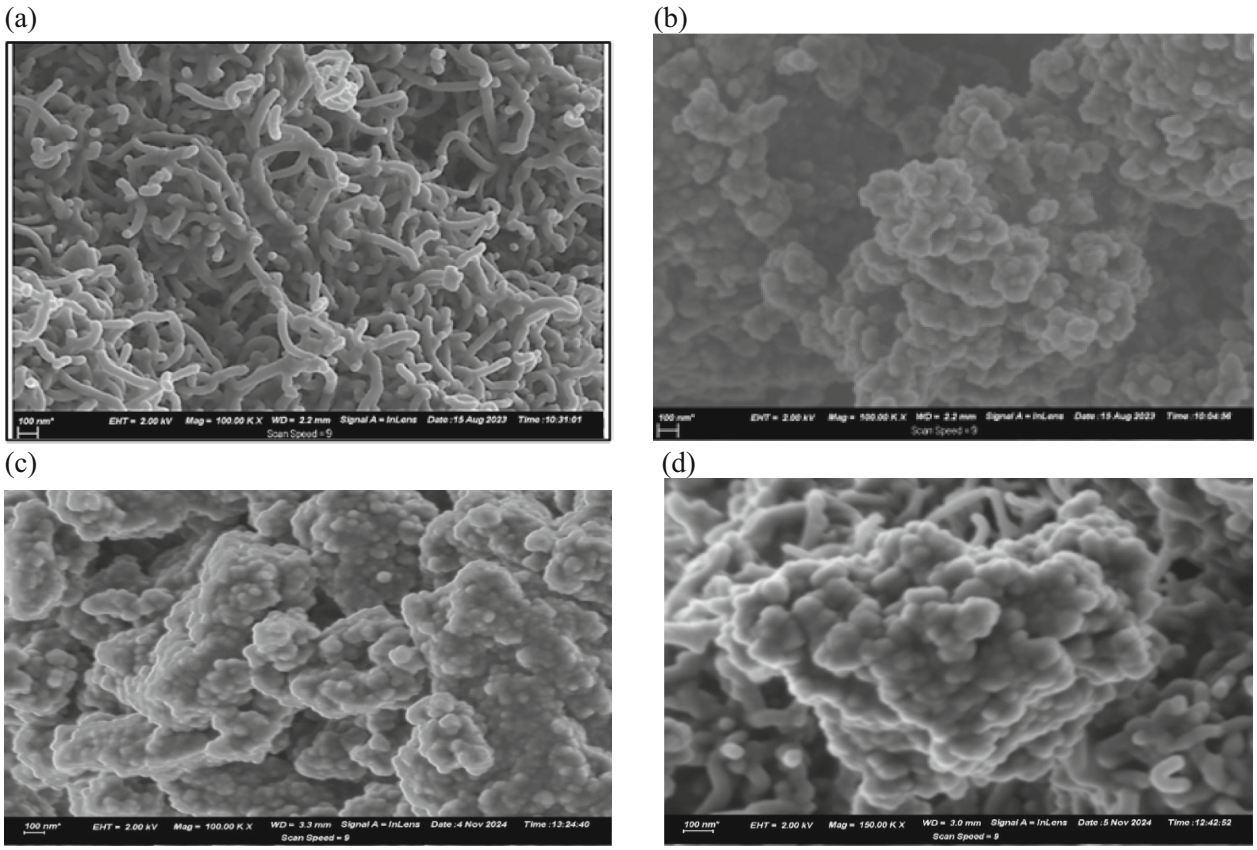

Fig. 4 SEM images of **a** MWCNT, **b** Al_2O_3, **c** Fe_3O_4, **d** Fe_3O_4/Al_2O_3/MWCNT at Magnification of 100KX

MWCNT content (Fig. 7c). Sample D (25% Fe_3O_4, 50% Al_2O_3, 25% MWCNT) achieved the highest EC, benefiting from the synergistic effects of both Fe_3O_4 and MWCNTs (Fig. 7d). Sample E (equal proportions) showed moderate EC, reflecting balanced contributions from both conductive and non-conductive components (Fig. 7e).

The enhancement in EC directly correlates with improved thermal conductivity, as the formation of conductive pathways facilitates efficient energy transfer. The magnetically responsive Fe_3O_4 also offers advantages in applications utilizing magnetic fields to promote fluid mixing and heat dispersion. Moreover, higher EC can support electrokinetic effects in electrically actuated microfluidic systems, potentially enhancing particle mobility and heat transfer.

Stability remains a crucial factor for practical application. Nanofluid stability, previously discussed in Sect. 3.3 and Table 3, reveals that higher Al_2O_3 content contributes to reduced sedimentation at low volume fractions, improving long-term dispersion. For example, Sample A and Sample E displayed higher sedimentation factor (SF) values at lower concentrations, confirming superior stability and reduced agglomeration. This balance between conductivity and colloidal stability is essential to prevent nanoparticle settling and ensure reliable performance over time.

Nonetheless, optimization of nanoparticle loading is vital. While increased Fe_3O_4 and MWCNT concentrations enhance EC, excessive loading may raise viscosity, reduce flowability, and accelerate sedimentation. Conversely, too low a concentration underutilizes the thermal and electrical benefits. Therefore, volume fractions between 0.00625% and 0.0125% are identified as optimal, offering a practical.

3.4.2 Variable sensitivity of THNF electrical conductivity

To evaluate the sensitivity of various features influencing the electrical conductivity (EC) of ternary hybrid nanofluids (THNF), five machine learning models Support Vector Machine (SVM) with a linear kernel, Random Forest, Gradient Boosting, Logistic Regression, and LightGBM were trained and tested using experimental data. Model performance was assessed based on classification accuracy, while feature importance was determined using permutation importance, as illustrated in Fig. 8a. The results indicate that Random Forest, Gradient Boosting, and LightGBM achieved high accuracy scores near 1.0, demonstrating their effectiveness in predicting EC. In contrast, the SVM model exhibited

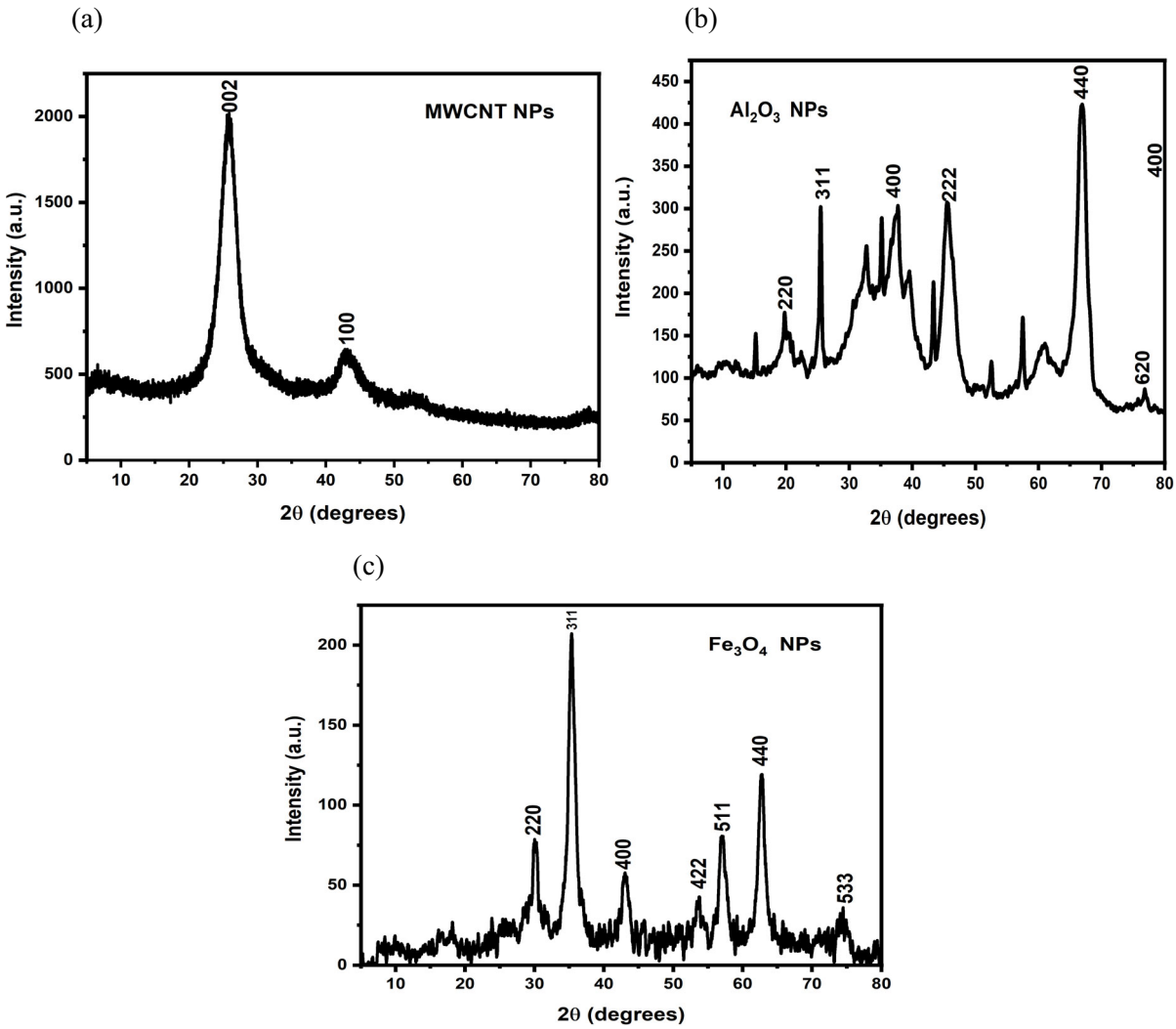

Fig. 5 Ternary nanoparticles, **a** MWCNT NPs, **b** Fe_3O_4 NPs, and **c** Al_2O_3 NPs

Table 3 Sedimentation factor (SF) for nanofluid samples A–E at varying volume fractions

Sedimentation factor							
Samples	0.3 vol%	0.2 vol%	0.1 vol%	0.05 vol%	0.025 vol%	0.0125 vol%	0.00625 vol%
A	12.392	38.431	59.775	73.736	82.165	86.921	89.562
B	11.322	26.50**9**	53.708	70.245	80.754	86.455	88.265
C	10.335	22.447	32.158	42.394	54.970	70.193	85.130
D	9.541	21.651	27.198	36.288	53.721	73.165	81.297
E	9.0401	18.689	24.718	38.051	42.548	69.552	74.020

lower accuracy, suggesting that the dataset's feature relationships do not conform well to a purely linear classification approach.

Feature importance analysis, shown in Fig. 8b, highlights the volume fraction (ϕ) as the most influential predictor of EC, particularly in the Gradient Boosting model. This suggests that variations in ϕ have a substantial impact on EC values. Temperature (T) demonstrates moderate importance, while the remaining features, Percentage Iron III Oxide Nanoparticles (F), Percentage Aluminum III Oxide Nanoparticles (A), and Percentage Multiwall Carbon Nanotube Nanoparticles (M) exhibit minimal influence. The LGBM model corroborates these findings, reinforcing that ϕ is the primary determinant of EC classification, with T

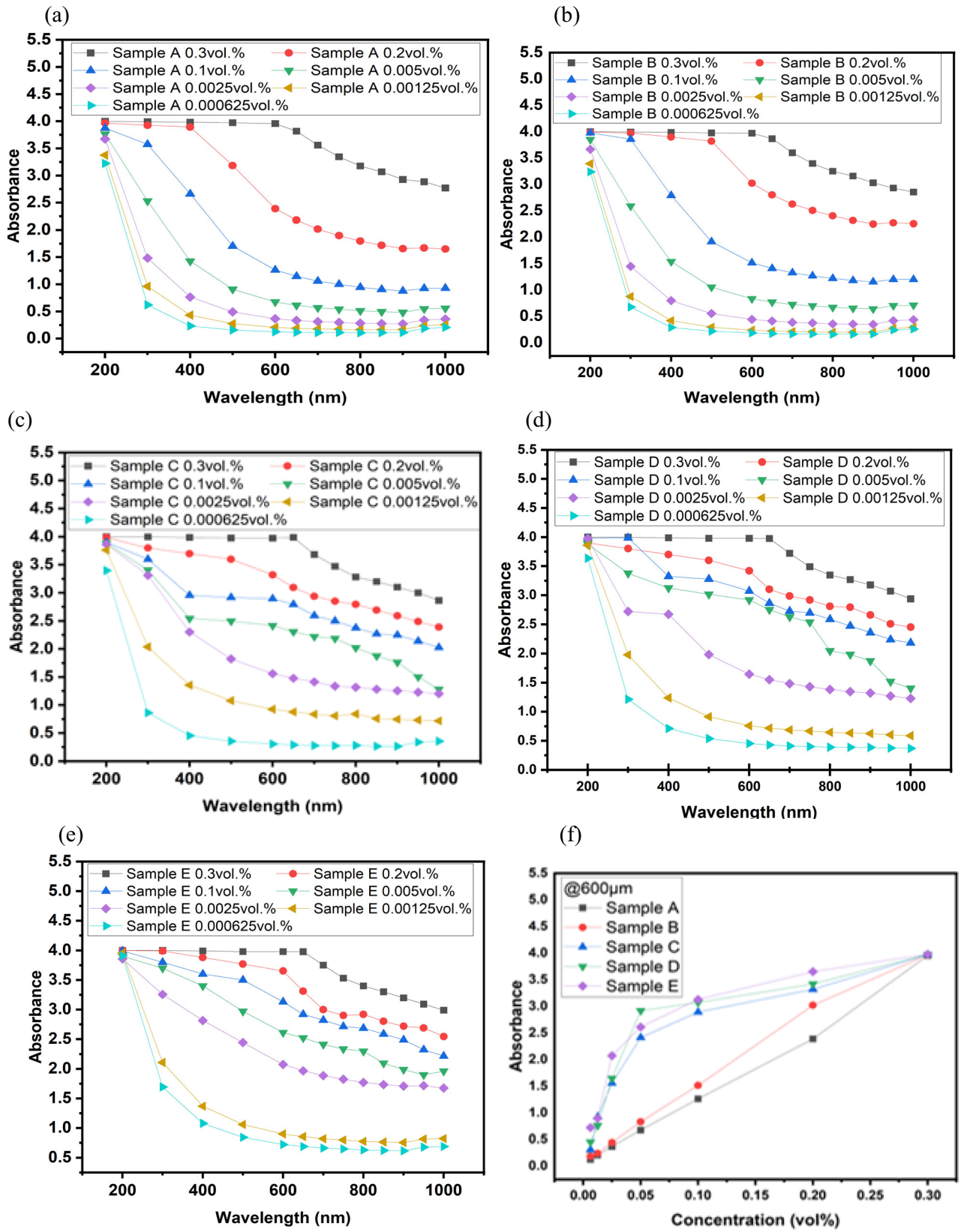

Fig. 6 SF for nanofluid stability **a** Sample A, **b** Sample B, **c** Sample C, **d** Sample D, **e** Sample E, and **f** Sample A–E with varied volume fractions @ 600 μm wavelength

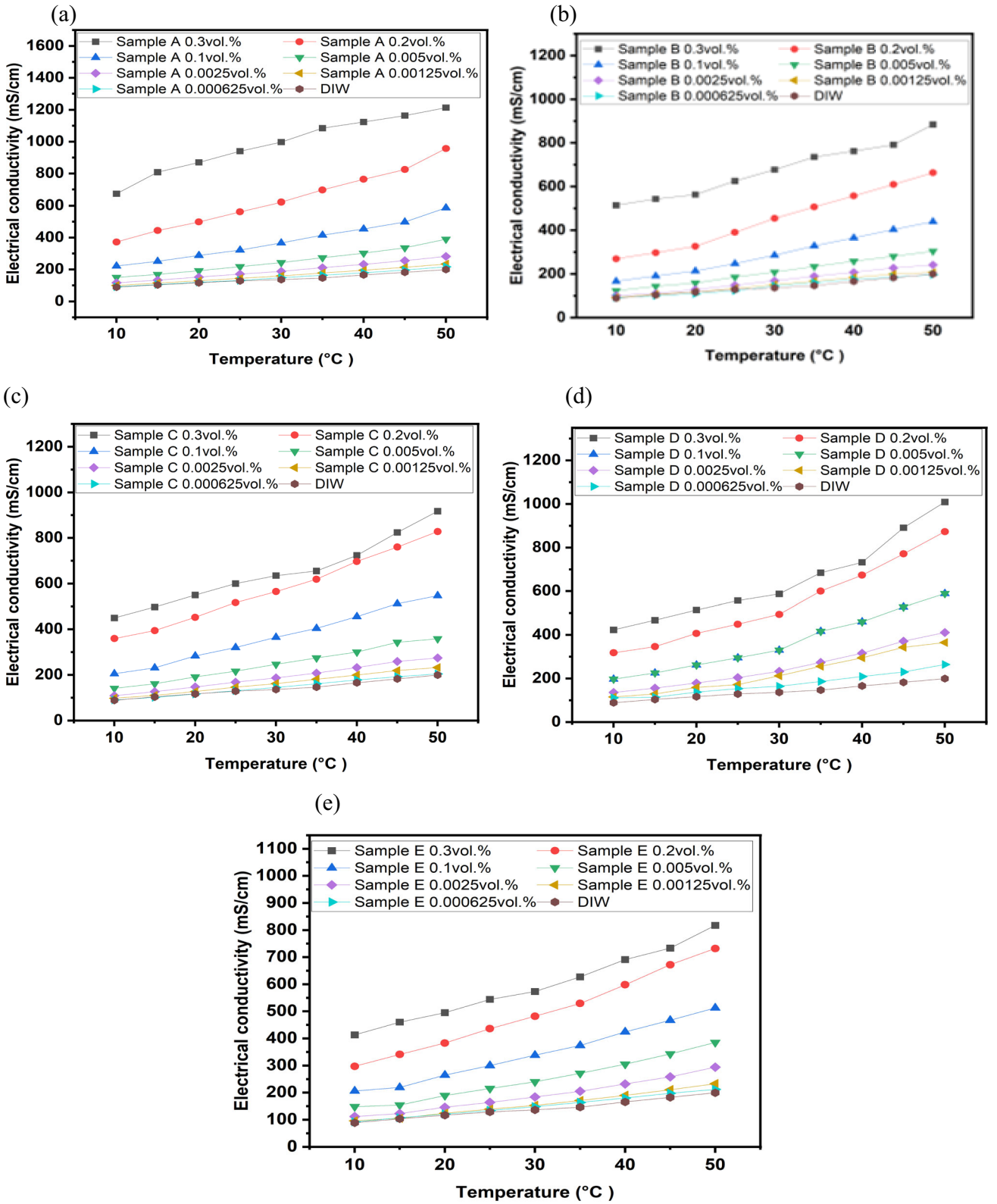

Fig. 7 Variation of EC with nanoparticle composition in Fe_3O_4/Al_2O_3/MWCNT with influence of temperature **a** Sample A, **b** Sample B, **c** Sample C, **d** Sample D, **e** Sample E

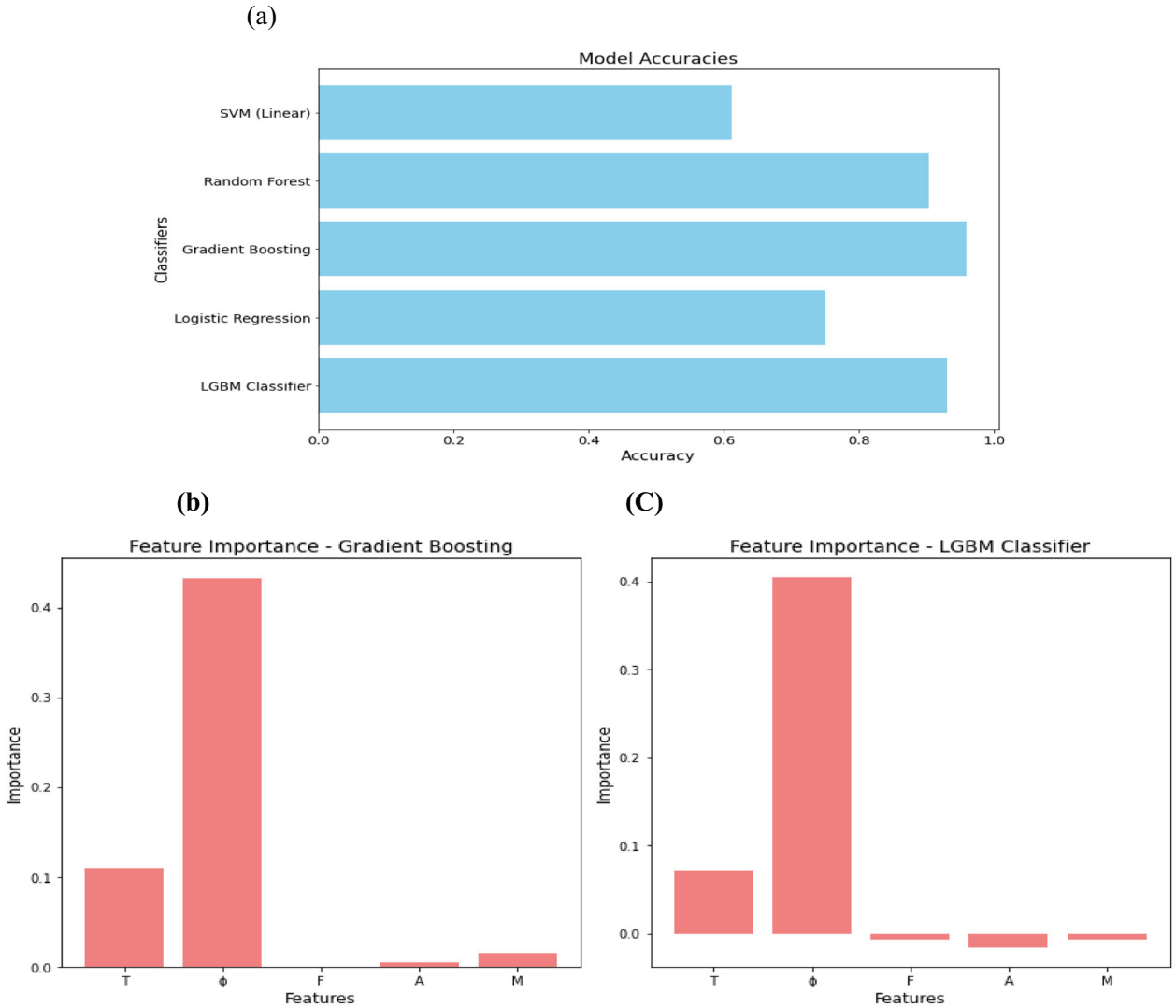

Fig. 8 **a** Accuracy of the different models for the EC, **b** feature importance plot for best classifiers of EC

playing a secondary role. The consistency between models strengthens the conclusion that ϕ is the dominant factor in predicting EC outcomes, whereas other features contribute to a lesser extent.

3.5 Effects of tri-hybrid nanoparticle composition and concentration on pH, stability, thermal performance, and their implications on thermal devices

3.5.1 Experimental results for pH of the nanofluids

The pH variation of Fe_3O_4/Al_2O_3/MWCNT hybrid nanofluids (Samples A–E) was evaluated as a function of temperature (10–50 °C) and volume fraction (0.000625–0.3%), with results shown in Fig. 9a–e. Across all samples, pH decreased with rising temperature and increased at lower volume fractions. Compared to deionized water (DIW), which maintained near-neutral pH values from 7.73 to 7.21, the nanofluids consistently exhibited lower, more acidic pH ranges.

Sample A (15% Fe_3O_4, 80% Al_2O_3, 5% MWCNT) exhibited a pH range of 6.19 to 4.35 (Fig. 9a), indicating acidic conditions at all test points. The acidity may pose corrosion concerns, though the dispersion remained stable and thermally efficient due to the synergistic effect of magnetic Fe_3O_4 and high-conductivity MWCNTs. Sample B (20% Fe_3O_4, 70% Al_2O_3, 10% MWCNT) followed a similar trend, with a pH of 6.75 to 4.54 (Fig. 9b), and enhanced thermal performance due to the increased conductive nanoparticle content, albeit with higher viscosity and sedimentation tendencies.

Sample C (20% Fe_3O_4, 60% Al_2O_3, 20% MWCNT) maintained pH values between 6.13 and 4.56 (Fig. 9c),

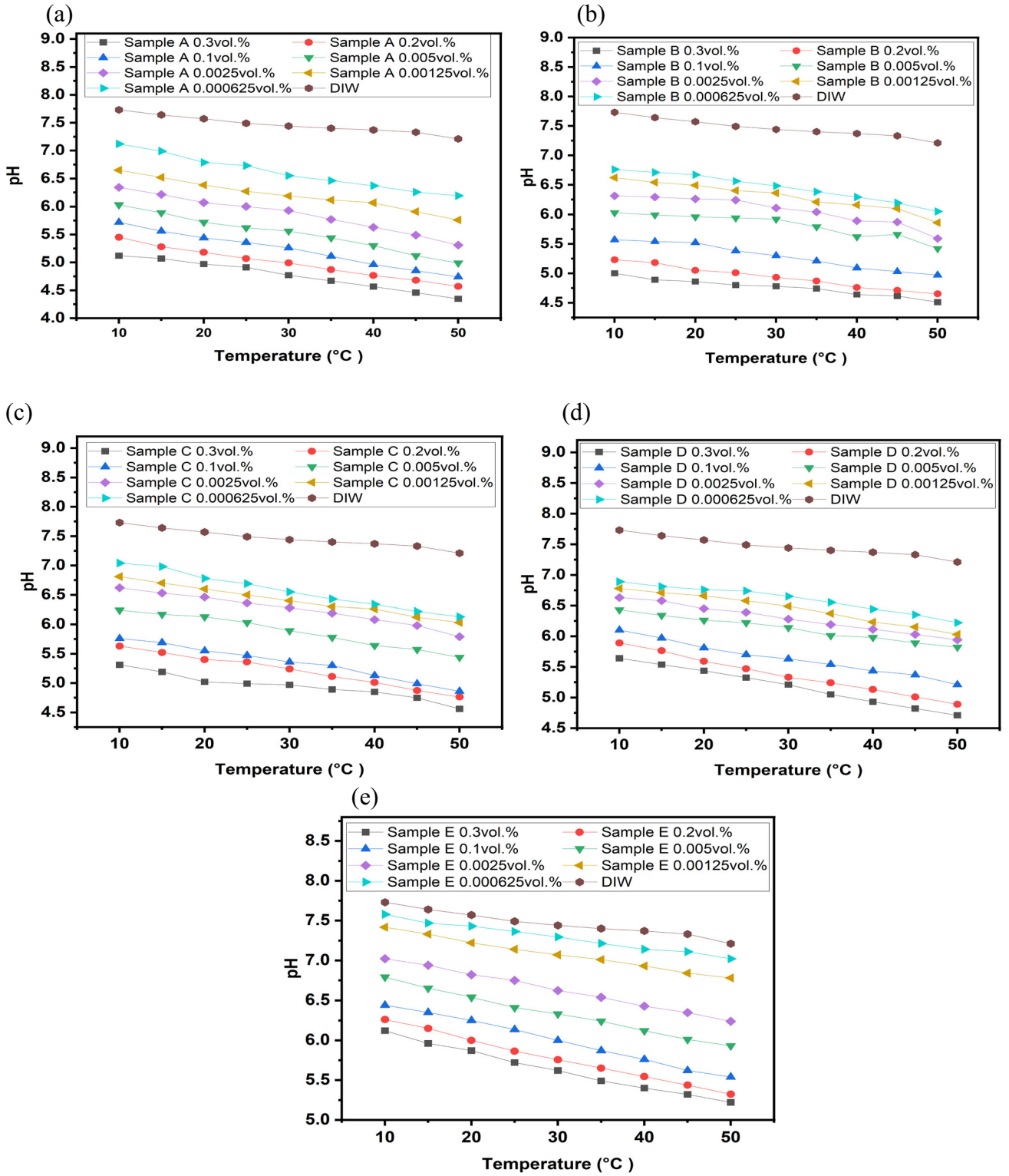

Fig. 9 Variation of pH with temperature and volume fraction for all samples compared to DIW **a** Sample A, **b** Sample B, **c** Sample C, **d** Sample D, **e** Sample E

reinforcing the observation that higher nanoparticle content improves heat transfer but may reduce dispersion stability. Sample D (25% Fe_3O_4, 50% Al_2O_3, 25% MWCNT) showed a pH range of 6.22 to 4.71 (Fig. 9d), demonstrating relatively balanced acidity with strong conductive potential. Sample E, with equal nanoparticle ratios (33.33% each), exhibited the highest pH among the nanofluids (7.02 to 5.22) (Fig. 9e), indicating comparatively lower acidity, though sedimentation and flow resistance remain concerns due to elevated solid content.

Fe_3O_4 nanoparticles contribute to acidity through iron ion leaching, particularly at higher concentrations. MWCNTs, depending on surface functionalization, may raise or stabilize pH, while Al_2O_3 has minimal direct pH impact but improves dispersion. The observed acidic behavior, especially at elevated temperatures and concentrations, underlines the need for corrosion mitigation and stability enhancement in practical applications.

To improve pH stability, surfactants like SDS or CTAB may be used to prevent flocculation by modifying surface charge. Buffering agents (e.g., phosphate or citrate systems) can help maintain near-neutral pH, while surface treatments (e.g., PEG or silica coatings) can reduce nanoparticle reactivity and prevent aggregation at higher temperatures. Additionally, careful hybridization ratio design can optimize thermal performance while minimizing sedimentation and viscosity.

In summary, increased Fe_3O_4 and MWCNT content improves thermal conductivity but induces acidic pH and risks related to corrosion, viscosity, and sedimentation. Proper pH management through chemical stabilization and nanoparticle surface modification is essential to ensure the long-term efficiency and reliability of these nanofluids in thermal systems.

3.5.2 Sensitivity analysis of pH in ternary hybrid nanofluids (THNF)

The influence of various features on the pH of ternary hybrid nanofluids (THNF) was analyzed using five machine learning models: Support Vector Machine (SVM) with a linear kernel, Random Forest, Gradient Boosting, Logistic Regression, and LightGBM. These models were trained and tested on experimental data, with classification accuracy used as the primary performance metric. Feature significance was assessed through permutation importance, as depicted in Fig. 10a. The results demonstrated that Random Forest, Gradient Boosting, Logistic Regression, and LightGBM achieved near-perfect accuracy, indicating their strong predictive capabilities for THNF pH. Conversely, SVM showed reduced accuracy, implying that the relationships among input features are not well captured by a strict linear approach.

As illustrated in Fig. 10b, feature importance analysis identified nanofluid volume fraction (ϕ) as the most critical determinant of pH, particularly in the Gradient Boosting and Logistic Regression models. This indicates that changes in ϕ substantially influence pH values. Temperature (T) was found to have a moderate effect, whereas the contributions of Iron (III) Oxide (F), Aluminum (III) Oxide (A), and Multi-wall Carbon Nanotubes (M) were minimal. Similar patterns were observed in the LightGBM model, further reinforcing the conclusion that ϕ plays a dominant role in pH prediction, with T having a secondary impact. The alignment of results across multiple models provides strong evidence that pH variations in THNF are primarily driven by ϕ, while other factors play a lesser role.

3.6 Influence of hybrid nanoparticle composition on viscosity (μ) and its implications for thermal management

3.6.1 Experimental results of nanofluids' viscosity

The viscosity and stability of Fe_3O_4/Al_2O_3/MWCNTs/DIW tri-hybrid nanofluids (THNFs) were assessed using a method adapted from Giwa et al. (2021), and Osman et al. (2019). As shown in Fig. 11, a data logger–connected viscometer recorded viscosity at 5-min intervals for 12 h immediately post-preparation at 25 °C and was repeated after one month. Samples A–E, all at 0.00125 vol.%, were selected based on their superior sedimentation stability. The observed consistency over one month affirms their long-term dispersion stability and suitability for thermal applications.

The impact of temperature and volume fraction on viscosity was further investigated and is presented in Fig. 12. Viscosity was found to decrease with rising temperature across all samples, as expected. At 10 °C, Sample E (33.3% each of Fe_3O_4, Al_2O_3, and MWCNTs) exhibited the highest viscosity (1.902 mPa·s at 0.3 vol.%), whereas DIW recorded the lowest (1.3059 mPa·s). At 50 °C, Sample E's viscosity reduced to 1.125 mPa·s, while DIW dropped to 0.5421 mPa·s. Volume fraction significantly influenced viscosity; Sample E at 0.3 vol.% showed a 45.6% increase over DIW, while Sample A (15% Fe_3O_4, 80% Al_2O_3, 5% MWCNTs) at 0.000625 vol.% showed only a 0.5% increase, underscoring the impact of nanoparticle loading.

The composition of the nanofluids notably influenced viscosity trends. Fe_3O_4 contributed magnetic responsiveness and moderate viscosity enhancement. Al_2O_3, being spherical and stable, had minimal impact on viscosity. MWCNTs, due to their high aspect ratio and network-forming behavior, dominated viscosity increase. As MWCNT content rose from 5 wt.% in Sample A to 25 wt.% in Sample D, viscosity increased accordingly due to nanotube entanglement. Sample A exhibited the lowest viscosity, favoring minimal pumping

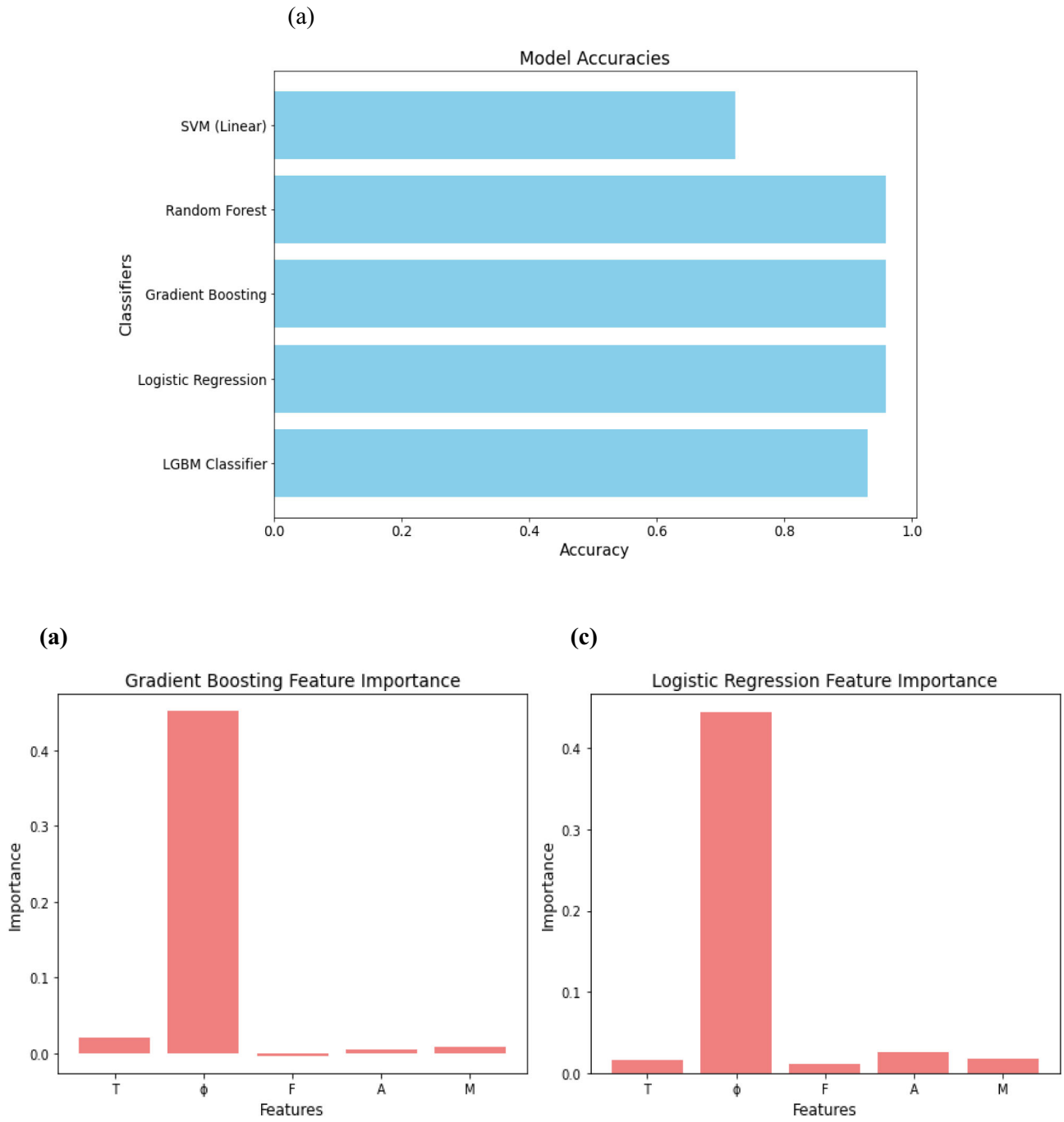

Fig. 10 **a** Accuracy of the different Models for the pH, **b** feature Importance plot for best Classifiers of pH

power, while Sample D showed the highest viscosity. Sample E showed intermediate behavior due to its balanced composition.

From a thermal systems design perspective, these results indicate that although higher MWCNT and nanoparticle concentrations enhance thermal conductivity, they also increase viscosity, requiring higher pumping energy. Samples B and C, with moderate MWCNT and Fe_3O_4 content, provide an optimal trade-off between thermal enhancement and acceptable flow resistance. Moreover, the inclusion of Fe_3O_4 offers potential for external magnetic field manipulation of flow behavior.

In conclusion, the viscosity of Fe_3O_4/Al_2O_3/MWCNT nanofluids is influenced by temperature, volume fraction, and composition, with MWCNT content being the most significant contributor. The long-term viscosity stability confirmed

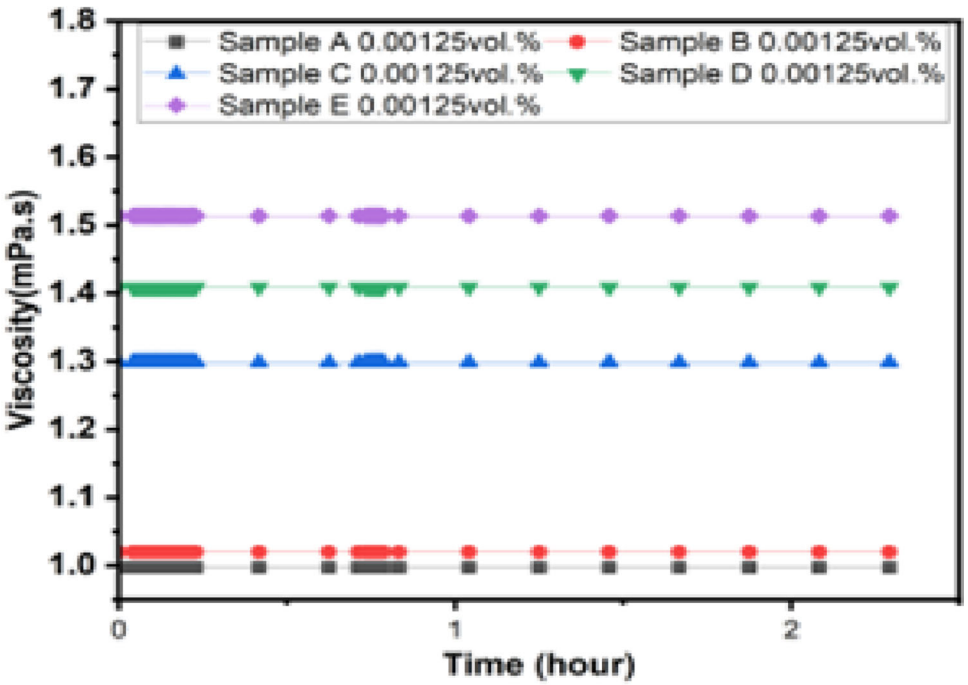

Fig. 11 Viscosity behavior and stability assessment of Fe_3O_4/Al_2O_3/MWCNTs/DIW THNFs at a 0.00125 vol% over time at 25 °C

by time-based measurements and the thermorheological trends suggest that Samples B and C are ideal candidates for practical thermal applications requiring both high heat transfer performance and manageable flow characteristics.

3.6.2 Sensitivity analysis and correlation modeling of viscosity in ternary hybrid nanofluids (THNF)

To investigate the key factors influencing the viscosity of ternary hybrid nanofluids (THNF), five machine learning algorithms; Support Vector Machine (SVM) with a linear kernel, Random Forest, Gradient Boosting, Logistic Regression, and LightGBM, were applied to experimental data. The models were assessed based on classification accuracy, and the relative importance of input features was determined using permutation-based analysis, as shown in Fig. 13a. Results indicated that Random Forest, Gradient Boosting, and LightGBM exhibited high predictive performance, achieving accuracy values close to 1.0. However, SVM and Logistic regression underperformed, suggesting that the complex nonlinear relationships between the input parameters are not effectively captured by a purely linear classification model.

Feature importance analysis, particularly in the Gradient Boosting and LightGBM models, as shown in Fig. 13b, identified temperature (T) as the most influential factor affecting nanofluid viscosity, followed by nanoparticle volume fraction (ϕ). Additionally, the mixing ratio of Aluminum (III) Oxide (A) exhibited a notable impact on viscosity, while Multiwall Carbon Nanotubes (M) had a moderate effect. In contrast, the influence of Iron (III) Oxide (F) was relatively minimal.

The correlation models developed for viscosity based on varying nanoparticle mixing ratios are summarized in Table 4. The coefficient of determination (R^2) values of 0.9788, 0.9642, and 0.8339 for samples A, B, and C indicate that viscosity variations are strongly influenced by T and ϕ, with predictive accuracies of approximately 98%, 96%, and 83%, respectively. In contrast, samples D and E demonstrated moderate predictive accuracy. Furthermore, the low mean square error (MSE) values, consistently below 0.04, confirm that the prediction errors are minimal, underscoring the robustness of the developed models.

3.7 Thermal conductivity (TC) and thermal management implications of THNFs

3.7.1 Experimental results of thermal conductivity of the nanofluids

The thermal conductivity (TC) of the Fe_3O_4/Al_2O_3/MWCNTs tri-hybrid nanofluids (THNFs) was experimentally evaluated across varying volume fractions and temperatures, as presented in Fig. 14. All nanofluid samples demonstrated a consistent increase in TC with rising temperature, indicating enhanced phonon activity and Brownian motion at elevated thermal levels. Notably, Sample A (15 wt.% Fe_3O_4, 80 wt.% Al_2O_3, 5 wt.% MWCNTs) showed a significant increase in TC from 0.61391 W/m·K at 10 °C to 0.70052 W/m·K at 50 °C, outperforming

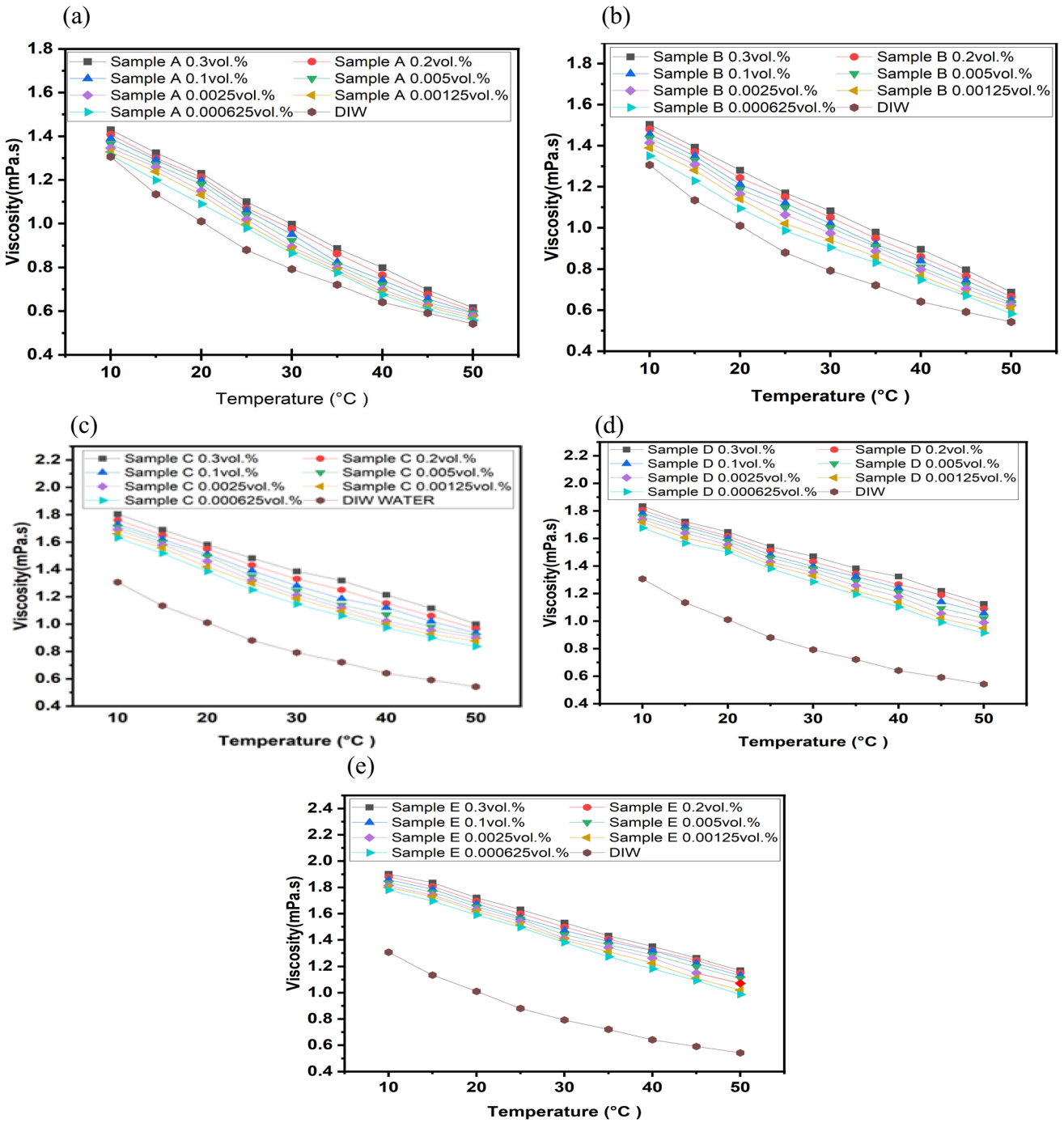

Fig. 12 Variation of viscosity with temperature and volume fraction for all samples compared to DIW **a** Sample A, **b** Sample B, **c** Sample C, **d** Sample D, **e** Sample E

other formulations and DIW. The enhancement stems from Fe_3O_4's magnetic thermal properties and MWCNTs' high intrinsic conductivity, while Al_2O_3 provided dispersion stability.

Sample B (20% Fe_3O_4, 70% Al_2O_3, 10% MWCNTs) achieved a peak TC of 0.68417 W/m·K at 50 °C. Though it contains more MWCNTs than Sample A, the reduced Fe_3O_4 content slightly compromised the thermal gain. Sample C (20% Fe_3O_4, 60% Al_2O_3, 20% MWCNTs) showed further improvement, reaching 0.69842 W/m·K, benefiting from the increased nanotube network, though balance remains crucial. Sample D (25% Fe_3O_4, 50% Al_2O_3, 25% MWCNTs) yielded 0.68331 W/m·K, but excessive solid loading may have reduced dispersion effectiveness. Sample E, equally

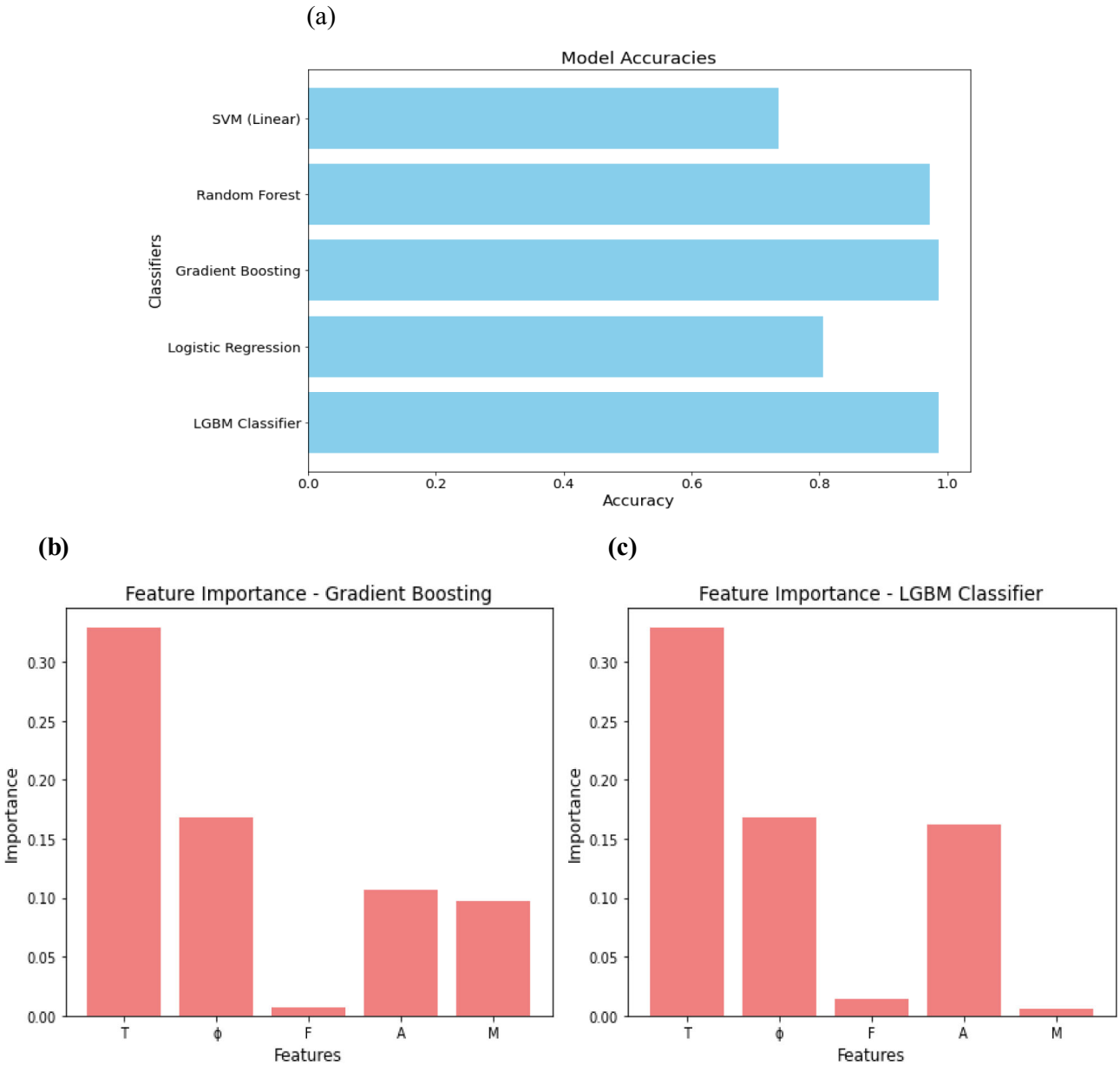

Fig. 13 **a** Accuracy of the different models for the viscosity, **b** feature importance plot for best classifiers of viscosity

Table 4 Viscosity correlations for THNF

Sample	Viscosity correlation	R2	MSE
A	$\mu = -0.0201(T) + 0.4104(\phi) + 1.5053$	0.9788	0.00149
B	$\mu = -0.0195(T) + 0.5656(\phi) + 1.5284$	0.9642	0.00249
C	$\mu = -0.0198(T) + 1.0178(\phi) + 1.7378$	0.8339	0.01522
D	$\mu = -0.0184(T) + 1.0381(\phi) + 1.7778$	0.7398	0.02384
E	$\mu = -0.0189(T) + 1.0378(\phi) + 1.8640$	0.6811	0.03315

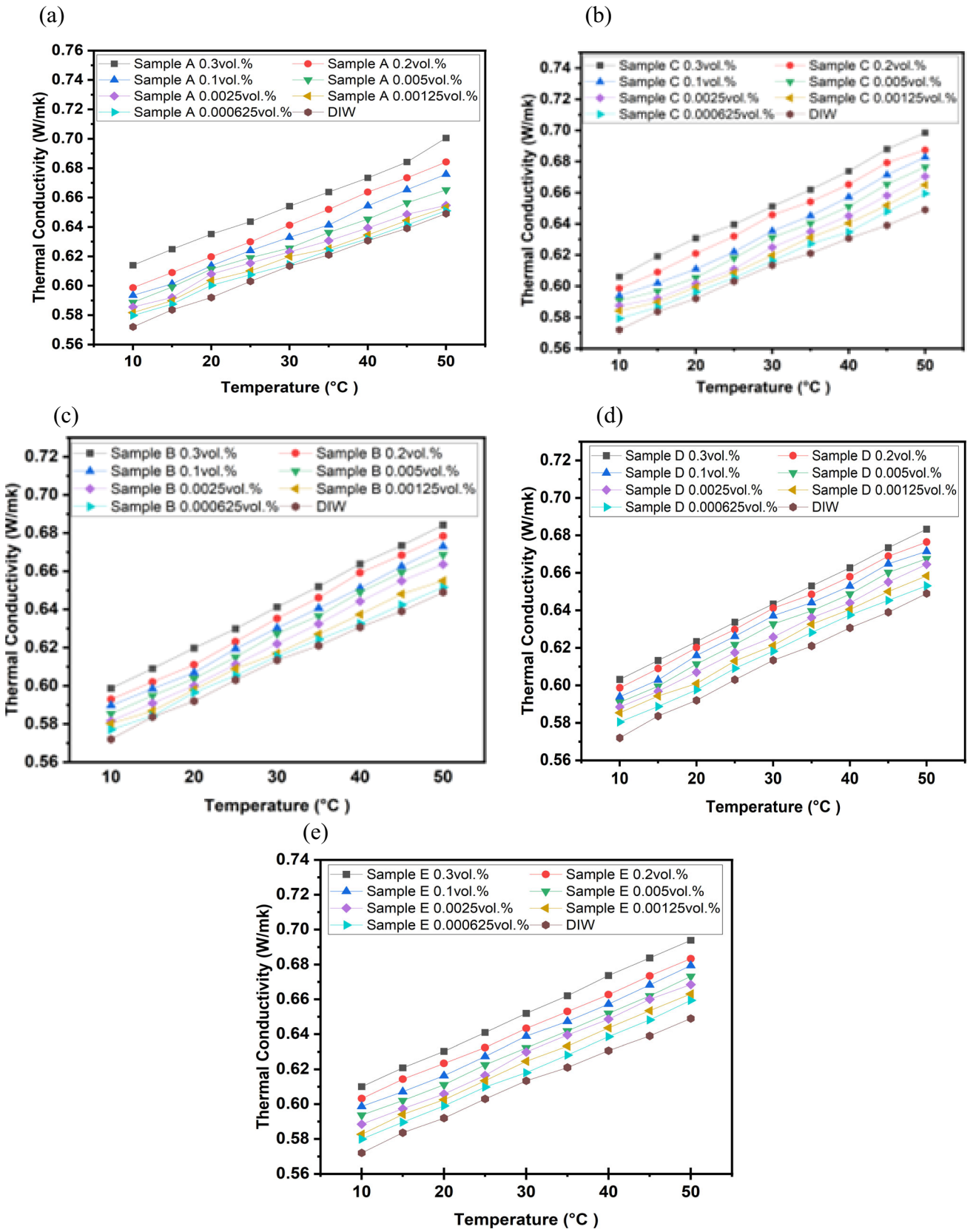

Fig. 14 Variation in TC of THNFs samples with different volume fractions compared to DIW **a** Sample A, **b** Sample B, **c** Sample C, **d** Sample D, **e** Sample E

composed of all three nanoparticles (33.33% each), maintained a stable TC of 0.69384 W/m·K, demonstrating the advantage of balanced hybridization for both conductivity and stability.

Despite thermal conductivity improvements at higher volume fractions, sedimentation observed in Table 3 indicates a trade-off. For instance, Sample A's sedimentation factor (SF) dropped from 89.56% at 0.00625% to 12.39% at 0.3%, confirming that greater nanoparticle concentrations reduce dispersion stability. This inverse relationship between TC and SF underscores that optimal thermal performance must balance nanoparticle loading and suspension stability.

In conclusion, although increased nanoparticle concentrations can elevate TC, excessive loading induces growth in viscosity and particle agglomeration, compromising long-term fluid performance. Lower volume fractions, specifically 0.00625% and 0.0125% were shown to provide the best compromise between thermal enhancement and colloidal stability. Among all samples, Sample A exhibited the most favorable combination of high TC and excellent dispersion, identifying it as the most effective candidate for thermal management applications. These findings reinforce that well-designed hybrid nanofluids, aided by proper hybridization ratios and stabilizing strategies, are critical for achieving reliable and efficient heat transfer performance and stability while reducing the risk of agglomeration and clogging. in advanced cooling systems.

3.7.2 Sensitivity analysis and correlation development of thermal conductivity in ternary hybrid nanofluids (THNF)

The thermal conductivity (TC) of ternary hybrid nanofluids (THNF) was systematically evaluated using five machine learning models: Support Vector Machine (SVM) with a linear kernel, Random Forest, Gradient Boosting, Logistic Regression, and LightGBM. These models were trained and tested on experimental data, with classification accuracy serving as the primary measure of performance. Feature significance was assessed using permutation importance, as illustrated in Fig. 15a. The results indicate that nearly all models exhibited high accuracy, demonstrating their strong predictive reliability for TC estimation in THNF.

Feature importance analysis, particularly in the Gradient Boosting and LightGBM models, presented in Fig. 15b, identified temperature (T) as the most dominant factor influencing nanofluid thermal conductivity, followed by nanoparticle volume fraction (ϕ). However, the specific mixing ratios of Iron (III) Oxide (F), Aluminum (III) Oxide (A), and Multiwall Carbon Nanotubes (M) had negligible effects on TC, suggesting that temperature and volume fraction primarily govern heat transfer behavior in THNF.

Table 5 summarizes the correlation models developed for TC based on different nanoparticle compositions. The obtained coefficient of determination (R^2) values exceeded 0.96 across all samples (A, B, C, D, and E), confirming that variations in TC are predominantly dictated by T and ϕ with exceptional predictive accuracy. Additionally, the mean square error (MSE) values remained below 0.000025, indicating minimal prediction errors and reinforcing the robustness of the developed models.

3.8 Influence of hybridization ratios on density, stability, and heat transfer efficiency of THNFs across temperature variation

The impact of hybridization ratios on the density and thermal behavior of Fe_3O_4/Al_2O_3/MWCNTs-based tri-hybrid nanofluids (THNFs) was examined across a range of temperatures, as shown in Fig. 16. The density of all nanofluids decreased with increasing temperature due to thermal expansion. Samples with higher Fe_3O_4 content such as Samples D (25 wt.% Fe_3O_4) and E (33.33 wt.% of each component), exhibited relatively slower density reduction, attributable to Fe_3O_4's thermal inertia and stabilizing effect. This trend reinforces the role of Fe_3O_4 in enhancing thermal stability and responsiveness under elevated temperatures.

Conversely, increasing MWCNT content across the samples improved nanoparticle dispersion and thermal conductivity due to their high aspect ratio and surface area. However, excessive MWCNT loading, as observed in Samples C and D, promoted agglomeration, which potentially compromised thermal performance and stability. Meanwhile, the gradual reduction in Al_2O_3 content, from 80 wt.% in Sample A to 50 wt.% in Sample D slightly diminished its stabilizing and conductive contributions, although Al_2O_3 maintained dispersion effectiveness across all samples.

From a thermal management standpoint, nanofluids with higher Fe_3O_4 content offer enhanced magnetic responsiveness, advantageous in externally modulated systems. However, this also increased viscosity, raising concerns about pumping energy. Although Sample E demonstrated a balanced composition and moderate density profile, its performance was suboptimal in terms of thermal conductivity due to sedimentation and viscosity buildup. Samples A and B, with lower MWCNT content and higher Al_2O_3 fractions, achieved better heat transfer efficiency and stability at minimal particle interactions. These findings emphasize that an optimized hybridization ratio favoring moderate Fe_3O_4 and MWCNT contentis crucial for achieving reliable, high-performance nanofluids suitable for advanced thermal systems.

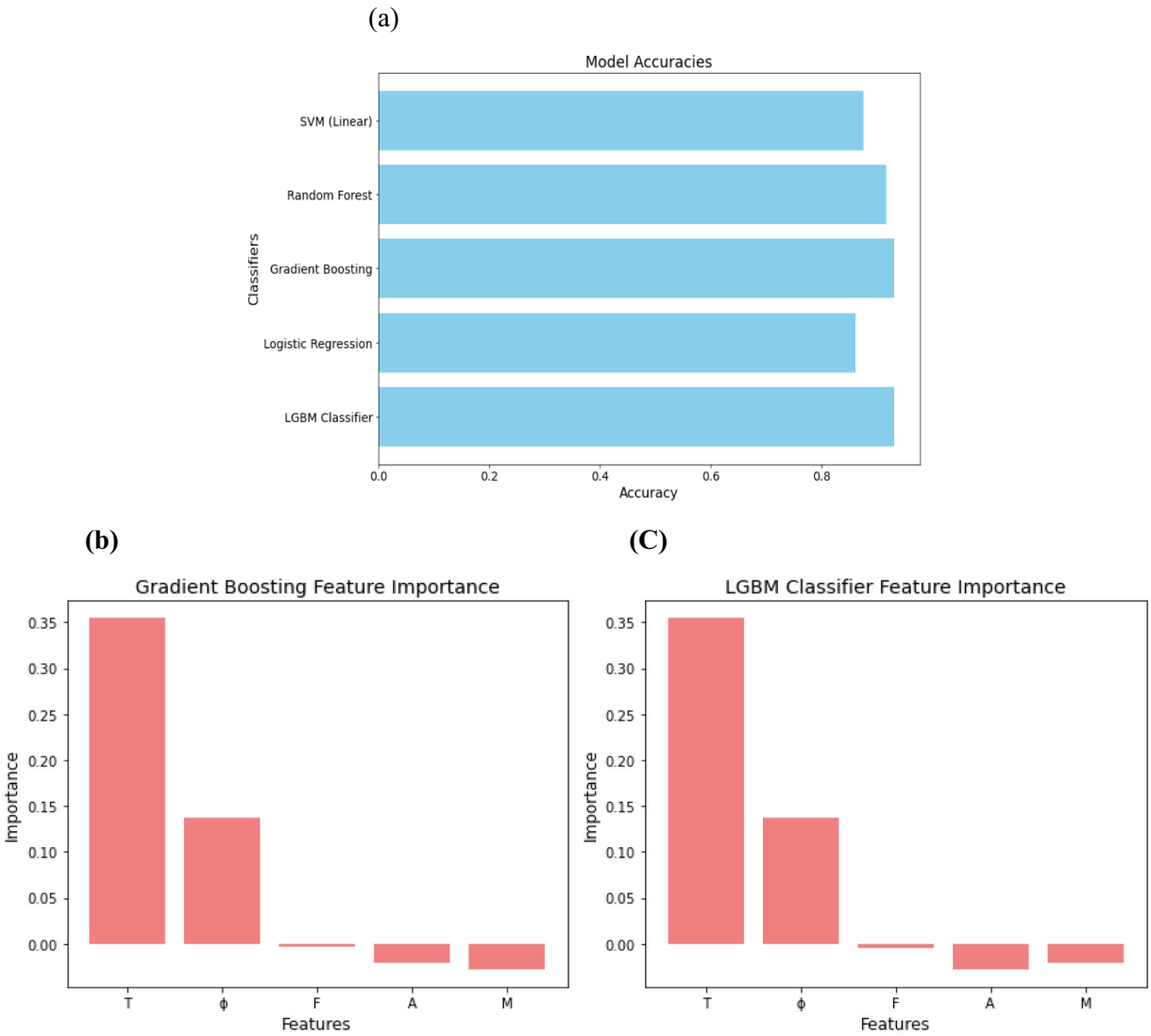

Fig. 15 **a** Accuracy of the different Models for the TC, **b** feature importance plot for best classifiers of TC

Table 5 Thermal conductivity correlations for THNF

Sample	Thermal conductivity correlation	R2	MSE
A	$K = 0.0019(T) + 0.1309(\phi) + 0.5592$	0.9817	0.000015
B	$K = 0.0020(T) + 0.0893(\phi) + 0.5558$	0.9783	0.000017
C	$K = 0.0021(T) + 0.1191(\phi) + 0.551$	0.9756	0.000023
D	$K = 0.0019(T) + 0.0882(\phi) + 0.563$	0.9679	0.000023
E	$K = 0.0020(T) + 0.1116(\phi) + 0.5611$	0.9699	0.000025

4 Conclusion

This study comprehensively evaluated the impact of hybridization ratios on the stability, thermophysical behavior, and magneto-hydrodynamic properties of Fe_3O_4/Al_2O_3/MWCNT tri-hybrid nanofluids (THNFs) for thermal applications. Key findings emphasize that careful optimization of hybrid composition directly influences dispersion stability, thermal conductivity (TC), electrical conductivity (EC), and heat transfer performance.

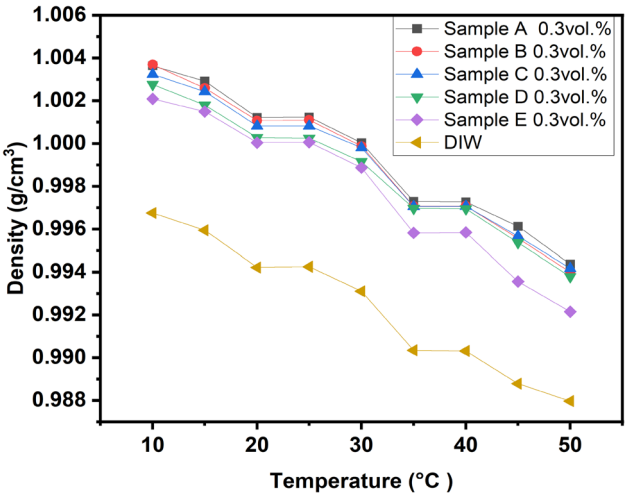

Fig. 16 Density variation of THNFs at different temperatures for various hybridization ratios of $\mathbf{Fe_3O_4}$, $\mathbf{Al_2O_3}$,and MWCNTs, compared to DIW

5 Key findings

i. **Stability and Sedimentation**: Sedimentation factor (SF) analysis revealed that higher Al_2O_3 content (e.g., Sample A with 80 wt.%) significantly improves dispersion stability by reducing agglomeration. Sample E (33.33 wt.% each) also showed favorable stability at low volume fractions. Al_2O_3's dispersive properties played a crucial role in minimizing long-term settling.

ii. **Electrical Conductivity and Magnetic Responsiveness**: Samples with increased Fe_3O_4 and MWCNT content, particularly Sample D (25 wt.% each), exhibited the highest EC due to synergistic effects from Fe_3O_4's magnetic and MWCNTs'conductive properties. These characteristics enhance heat transfer and enable control under external magnetic fields.

iii. **Thermal Conductivity and Heat Transfer**: TC increased with temperature and nanoparticle content. MWCNTs facilitated efficient heat transfer through their high-aspect-ratio network structure, while Fe_3O_4 contributed magnetic functionality. However, excess MWCNTs (Samples C and D) led to aggregation, reducing stability and TC. Sample E offered the best compromise between TC, stability, and viscosity.

iv. **Density and Viscosity Behavior**: THNFs demonstrated temperature-dependent density reduction, with Fe_3O_4-rich samples (D, E) maintaining thermal stability. Viscosity decreased with temperature but increased at higher volume fractions, highlighting the importance of low-volume concentrations (0.00625–0.0125 vol.%) for efficient heat transfer with minimal flow resistance.

v. **pH Stability and Corrosion Consideration**: All nanofluids remained acidic, with decreasing pH at elevated temperatures and concentrations, posing potential corrosion risks. Mitigation strategies such as the addition of surfactants (e.g., SDS, CTAB), buffers, or surface functionalization (e.g., PEG, silica coatings) are recommended.

vi. **Machine Learning Validation**: Predictive modeling using Random Forest, Gradient Boosting, and LightGBM demonstrated excellent accuracy ($R^2 > 0.96$) for viscosity and TC. Temperature (T) was the most influential feature, while volume fraction (ϕ) predominantly affected pH and EC. Extremely low mean squared error values (< 0.000025) confirm model reliability.

vii. **Practical Implication**: The tri-hybrid formulation enables enhanced EC, tunable viscosity, and improved TC, making it suitable for applications such as electronic cooling, magnetic heat exchangers, microfluidic devices, and energy systems. Sample E's balanced hybrid ratio offers optimal performance under varied operating conditions, though the trade-offs between viscosity, stability, and TC must be carefully managed.

Further research can explore:

i. Tailoring nanoparticle ratios to meet application-specific thermal and electrical demands.
ii. Leveraging magnetic and electrokinetic phenomena for active flow control.
iii. Integrating pH buffers and surfactants to enhance long-term dispersion stability.
iv. Testing system-level performance of THNFs in real-world thermal management environments.

In summary, Fe_3O_4/Al_2O_3/MWCNT-based THNFs present a promising pathway for next-generation heat transfer fluids, offering a versatile combination of thermal performance, magnetic control, and tunable rheological properties.

Acknowledgements The authors would like to express their gratitude to the Microscopy Department of the University of Pretoria for providing access to the equipment and facilities necessary for conducting the morphology and XRD imaging analyses. Their support was instrumental in completing this research.

Author contribution Victor Omoefe Adogbeji: Involved in gathering data, conducting experiments, validating results, analyzing findings, and preparing the initial draft of the manuscript. Emmanuel O. Atofarati: Involved in data capturing, conducting experiments, validating results, analysing findings, and preparing the initial draft of the manuscript. Kuvendran Govinder: Contributed to data collection, experimental procedures, result validation, data analysis, and drafting the initial manuscript. Mohsen Sharifpur: Contributed to the research design, validation processes, manuscript development and revisions, supervised the study, and obtained financial support for the project. Joshua P.

Meyer: Assisted in refining the methodology, reviewing and revising the manuscript, and co-supervised the project.

Funding Open access funding provided by University of Pretoria.

Data availability No datasets were generated or analysed during the current study.

Declarations

Competing interests The authors declare no competing interests.

References

Adio SA et al (2025) Nanofluids flow boiling and convective heat transfer in microchannels: a systematic review and bibliometrics analysis. J Therm Anal Calorim 2025:1–33. https://doi.org/10.1007/S10973-025-14265-X

Adogbeji VO, Sharifpur M, Meyer JP (2025b) International journal of thermal sciences experimental investigation of heat transfer, thermal efficiency, pressure drop, and flow characteristics of Fe_3O_4-MgO magnetic hybrid nanofluid in transitional flow regimes. Int J Therm Sci 209:109515. https://doi.org/10.1016/j.ijthermalsci.2024.109515

Adogbeji VO, Atofarati EO, Sharifpur M, Meyer JP (2025) Results in physics magnetohydrodynamics of nanofluid internal forced convection : a review and outlook for practical applications. Results Phys 68:108082. https://doi.org/10.1016/j.rinp.2024.108082

Adogbeji VO, Sharifpur M, Meyer JP (2024) Case studies in thermal engineering experimental investigation of heat transfer enhancement , thermal efficiency , and pressure drop in forced convection of magnetic hybrid nanofluid (Fe_3O_4/TiO_2) under varied magnetic field strengths and waveforms. Case Stud Therm Eng 63:105313. https://doi.org/10.1016/j.csite.2024.105313

Adogbeji VO, Sharifpur M, Meyer JP (2025) Experimental investigation into heat transfer and flow characteristics of magnetic hybrid nanofluid (Fe_3O_4/TiO_2) in turbulent region. Appl Therm Eng 258:124630. https://doi.org/10.1016/j.applthermaleng.2024.124630

Adogbeji VO, Atofarati EO, Sharifpur M, Meyer JP (2025) Experimental investigation and machine learning modelling of the effects of hybridization mixing ratio, nanoparticle type, and temperature on the thermophysical properties of Fe_3O_4/TiO_2, Fe_3O_4/MgO, and Fe_3O_4/ZnO DI water hybrid ferrofluids. J Therm Anal Calorim

Adun H, Kavaz D, Wole-Osho I, Dagbasi M (2021) Synthesis of Fe_3O_4-Al_2O_3-ZnO/water ternary hybrid nanofluid: investigating the effects of temperature, volume concentration and mixture ratio on specific heat capacity, and development of hybrid machine learning for prediction. J Energy Storage 41:102947. https://doi.org/10.1016/j.est.2021.102947

Ahmad S et al (2023) Localized magnetic fields and their effects on heat transfer enhancement and vortices generation in tri-hybrid nanofluids: a novel investigation. Case Stud Therm Eng 50:103408. https://doi.org/10.1016/j.csite.2023.103408

Aravind SSJ, Baskar P, Baby TT, Sabareesh RK, Das S, Ramaprabhu S (2011) Investigation of structural stability, dispersion, viscosity, and conductive heat transfer properties of functionalized carbon nanotube based nanofluids. J Phys Chem C 115(34):16737–16744. https://doi.org/10.1021/jp201672p

Arifutzzaman A, Ismail AF, Yaacob II, Alam MZ, Khan AA (2019) Stability investigation of water based exfoliated graphene nanofluids. IOP Conf Ser Mater Sci Eng 488(1). https://doi.org/10.1088/1757-899X/488/1/012002

Atofarati EO, Sharifpur M, Huan Z, Awe OO, Meyer JP (2025) Experimental and machine learning study on the influence of nanoparticle size and pulsating flow on heat transfer performance in nanofluid-jet impingement cooling. Appl Therm Eng 258:124631. https://doi.org/10.1016/J.APPLTHERMALENG.2024.124631

Atofarati EO, Sharifpur M, Meyer JP (2024) Pulsating nanofluid-jet impingement cooling and its hydrodynamic effects on heat transfer. Int J Therm Sci 198:108874. https://doi.org/10.1016/j.ijthermalsci.2023.108874

Çengel J, Yunus A, Ghajar A (2020) Heat and mass transfer in SI units: fundamentals and applications (6th ed). MCGraw Hill

Chakraborty S, Sarkar I, Ashok A, Sengupta I, Pal SK, Chakraborty S (2018a) Thermo-physical properties of Cu-Zn-Al LDH nanofluid and its application in spray cooling. Appl Therm Eng 141(May):339–351. https://doi.org/10.1016/j.applthermaleng.2018.05.114

Chakraborty S, Sarkar I, Ashok A, Sengupta I, Pal SK, Chakraborty S (2018b) Synthesis of Cu-Al LDH nanofluid and its application in spray cooling heat transfer of a hot steel plate. Powder Technol 335:285–300. https://doi.org/10.1016/j.powtec.2018.05.004

Chakraborty S, Panigrahi PK (2020) Stability of nanofluid: a review. Applied Thermal Eng 174. https://doi.org/10.1016/j.applthermaleng.2020.115259

Choi SUS, Eastman JA (1995) Enhancing thermal conductivity of fluids with nanoparticles. ASME Int Mech Eng Fluids Eng Div FED 8(231):99–105. https://doi.org/10.1021/je60018a001

Das SK, Choi SUS, Patel HE (2006) Heat transfer in nanofluids—a review. Heat Transfer Eng 27(10):3–19. https://doi.org/10.1080/01457630600904593

Giwa SO, Sharifpur M, Ahmadi MH, Sohel Murshed SM, Meyer JP (2021) Experimental investigation on stability, viscosity, and electrical conductivity of water-based hybrid nanofluid of mwcnt-fe2o3. Nanomaterials 11(1):1–19. https://doi.org/10.3390/nano11010136

Hamilton R, Crosser O (1962) Thermal conductivity of heterogeneous two-component systems, no 1, pp 1887–1891

Kanti P, Sharma KV, Khedkar RS, Ur Rehman T (2022) Synthesis, characterization, stability, and thermal properties of graphene oxide based hybrid nanofluids for thermal applications: experimental approach. Diam Relat Mater 128:109265. https://doi.org/10.1016/J.DIAMOND.2022.109265

Kanti PK, Sharma P, Wanatasanappan VV, Said NM (2024) Explainable machine learning techniques for hybrid nanofluids transport characteristics: an evaluation of shapley additive and local interpretable model-agnostic explanations. J Therm Anal Calorim 149(21):11599–11618. https://doi.org/10.1007/S10973-024-13639-X/FIGURES/14

Khedaer Z, Ahmed D, Al-Jawad S (2021) Investigation of morphological, optical, and antibacterial properties of hybrid ZnO-MWCNT prepared by sol-gel. J Appl Sci Nanotechnol 1(2):66–77. https://doi.org/10.53293/jasn.2021.11634

Kline SJ (1985) The purposes of uncertainty analysis. Trans ASME 107:154

Kulkarni DP, Namburu PK, Ed Bargar H, Das DK (2008) Convective heat transfer and fluid dynamic characteristics of SiO_2—ethylene glycol/water nanofluid. Heat Transf Eng 29(12):1027–1035. https://doi.org/10.1080/01457630802243055

Maxwell JC (1891) A treatise on electricity and magnetism, clarendon. Oxford, UK, p 1891

Mehrali M et al (2014) Preparation, characterization, viscosity, and thermal conductivity of nitrogen-doped graphene aqueous nanofluids. J Mater Sci 49(20):7156–7171. https://doi.org/10.1007/s10853-014-8424-8

Moffat RJ (1988) Describing the uncertainties in experimental results. Exp Therm Fluid Sci 1(1):3–17. https://doi.org/10.1016/0894-1777(88)90043-X

Mohammed AA, Khodair ZT, Khadom AA (2020) Preparation and investigation of the structural properties of α-Al2O3 nanoparticles using the sol-gel method. Chem Data Collect 29:100531. https://doi.org/10.1016/j.cdc.2020.100531

Mousavi SM, Esmaeilzadeh F, Wang XP (2019) Effects of temperature and particles volume concentration on the thermophysical properties and the rheological behavior of CuO/MgO/TiO_2 aqueous ternary hybrid nanofluid: experimental investigation. J Therm Anal Calorim 137(3):879–901. https://doi.org/10.1007/s10973-019-08006-0

Muzaidi NAS et al (2021) Heat absorption properties of CuO/TiO_2/SiO_2 trihybrid nanofluids and its potential future direction towards solar thermal applications. Arab J Chem 14(4):103059. https://doi.org/10.1016/j.arabjc.2021.103059

Okonkwo EC, Wole-Osho I, Almanassra IW, Abdullatif YM, Al-Ansari T (2021) An updated review of nanofluids in various heat transfer devices. J Therm Anal Calorimetry 145(6):2817–2872. https://doi.org/10.1007/s10973-020-09760-2

Osman S, Sharifpur M, Meyer JP (2019) Experimental investigation of convection heat transfer in the transition flow regime of aluminium oxide-water nanofluids in a rectangular channel. Int J Heat Mass Transf 133:895–902. https://doi.org/10.1016/j.ijheatmasstransfer.2018.12.169

Ramadhan AI, Azmi WH, Mamat R, Hamid KA, Norsakinah S (2019) Investigation on stability of tri-hybrid nanofluids in water-ethylene glycol mixture. IOP Conf Ser Mater Sci Eng 469(1). https://doi.org/10.1088/1757-899X/469/1/012068

Ramadhan AI, Azmi WH, Mamat R (2020) Heat transfer characteristics of car radiator using tri-hybrid nanocoolant. IOP Conf Ser Mater Sci Eng 863(1). https://doi.org/10.1088/1757-899X/863/1/012054

Sahoo RR (2020) Experimental study on the viscosity of hybrid nanofluid and development of a new correlation. Heat Mass Transf und Stoffuebertragung 56(11):3023–3033. https://doi.org/10.1007/s00231-020-02915-9

Sepehrnia M, Shahsavar A, Maleki H, Moradi A (2023) Experimental study on the dynamic viscosity of hydraulic oil HLP 68-Fe_3O_4-TiO_2-GO ternary hybrid nanofluid and modeling utilizing machine learning technique. J Taiwan Inst Chem Eng 145:104841. https://doi.org/10.1016/J.JTICE.2023.104841

Sepehrnia M, Maleki H, Forouzandeh Behbahani M (2023) Tribological and rheological properties of novel MoO3-GO-MWCNTs/5W30 ternary hybrid nanolubricant: experimental measurement, development of practical correlation, and artificial intelligence modeling. Powder Technol 421:118389. https://doi.org/10.1016/J.POWTEC.2023.118389

Sepehrnia M, Davoodabadi Farahani S, Hamidi Arani A, Taghavi A, Golmohammadi H (2023) Laboratory investigation of GO-SA-MWCNTs ternary hybrid nanoparticles efficacy on dynamic viscosity and wear properties of oil (5W30) and modeling based on machine learning. Sci Rep 13(1):1–18. https://doi.org/10.1038/s41598-023-37623-x

Shahsavar A, Sepehrnia M, Maleki H, Darabi R (2023) Thermal conductivity of hydraulic oil-GO/Fe_3O4/TiO_2 ternary hybrid nanofluid: experimental study, RSM analysis, and development of optimized GPR model. J Mol Liq 385:122338. https://doi.org/10.1016/J.MOLLIQ.2023.122338

Shahsavar A, Sepehrnia M, Fateh Moghaddam A, Davoodabadi Farahani S (2024) Effects of sonication time on thermophysical properties of ternary hybrid nanofluid and modeling thermophysical properties utilizing two GMDH and SVR models based on machine learning. J Taiwan Inst Chem Eng 163:105650. https://doi.org/10.1016/J.JTICE.2024.105650

Sun Y et al (2020) Properties of nanofluids and their applications in enhanced oil recovery: a comprehensive review. Energy Fuels 34(2):1202–1218. https://doi.org/10.1021/acs.energyfuels.9b03501

Timofeeva EV, Yu W, France DM, Singh D, Routbort JL (2011) Nanofluids for heat transfer: an engineering approach. Nanoscale Res Lett 6(1):1–7. https://doi.org/10.1186/1556-276X-6-182

Vicki Wanatasanappan V, Kumar Kanti P, Sharma P, Husna N, Abdullah MZ (2023) Viscosity and rheological behavior of Al_2O_3-Fe_2O_3/water-EG based hybrid nanofluid: a new correlation based on mixture ratio. J Mol Liq 375:121365. https://doi.org/10.1016/j.molliq.2023.121365

Wole-osho I, Okonkwo EC, Abbasoglu S, Kavaz D (2020) Nanofluids in solar thermal collectors: review and limitations, vol 41, no 11. Springer US. https://doi.org/10.1007/s10765-020-02737-1

Zhuang L, Zhang W, Zhao Y, Shen H, Lin H, Liang J (2015) Preparation and characterization of Fe_3O_4 particles with novel nanosheets morphology and magnetochromatic property by a modified solvothermal method. Sci Rep 5:1–6. https://doi.org/10.1038/srep09320

Zubir MNM et al (2015) Experimental investigation on the use of reduced graphene oxide and its hybrid complexes in improving closed conduit turbulent forced convective heat transfer. Exp Therm Fluid Sci 66:290–303. https://doi.org/10.1016/j.expthermflusci.2015.03.022